UiO : Department of Physics
University of Oslo

Advanced Modelling of NiMH Batteries

Integrating Renewable Energy Sources into EV Charging Stations

Morten Østigård

Master's Thesis, Spring 2019

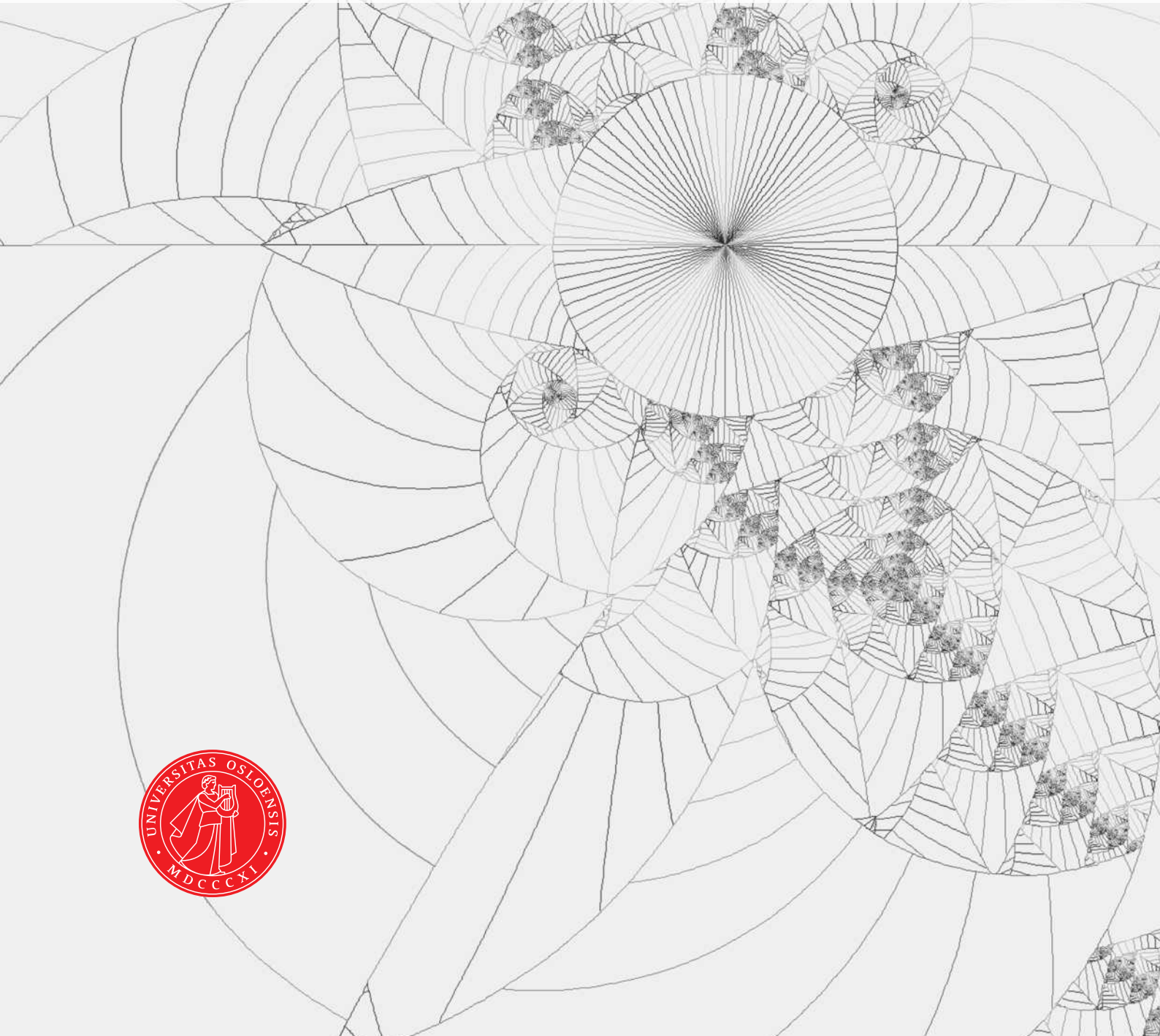

Advanced Modelling of NiMH Batteries: Integrating Renewable Energy Sources into EV Charging Stations

by

Morten Østigård

Thesis submitted for the degree of
Master of Science in Materials Science and Nanotechnology
60 credits

University of Oslo

Spring 2019

Abstract

This thesis is devoted to the topic of energy storage system modelling, and to the integration of such systems to increase the utilisation of renewable energy. In particular, the use of a nickel-metal hydride battery storage system is considered in combination with energy produced by solar and wind to power an electric vehicle fast-charging station situated in Norway.

The thesis aims to develop a flexible model for the battery energy storage system that can accurately describe battery performance and performance-reducing effects. The motivation of which is to be able to evaluate the feasibility of the charging topology in mention.

A semi-empirical, battery model based on real data is designed and implemented in the Simulink modelling environment. Further, a system model is developed in the same modelling environment which uses actual data from Norwegian renewable energy producers and charging station operators. We report on the influence of renewable energy mixture, capacity sizing, production sizing and vehicle charging behaviour on the feasibility of the topology.

The thesis is written as a contribution of the now finished project INTEGRARE (Intelligent prediction and integration of renewable energy sources into the Norwegian electricity grid, headed by the Department of Technology Systems). The topic is in line with an ongoing effort in the energy storage system research group to promote, design, model and validate the feasibility of energy systems powered by renewable energy sources.

Saving our planet, lifting people out of poverty,
advancing economic growth; these are one and the same fight.
We must connect the dots between climate change, water scarcity,
energy shortages, global health, food security and women's empowerment.
Solutions to one problem must be solutions for all.
— Ban Kimoon

Acknowledgments

First, and foremost, I would like to express sincere gratitude to my primary supervisor, associate professor Sabrina Sartori, for her guidance and support. We might not always have been in the same time zone, but you were always available when I needed your input. Secondly, I would like to thank my other supervisor, Øystein Ulleberg, for his insight on energy systems modelling and fruitful discussions about applications. I am also in debt to Mohsen Vatani at Institute for Energy Technology and Amin Hajizadeh at Aalborg University for providing support on using Simulink, and to Anette Eleonora Gunnæs for proofreading this thesis.

I wish to thank the structure physics group at the University of Oslo for providing excellent office facilities throughout these two years, for Friday beers and off-topic discussions in the coffee room. Even though I was never officially part of your group, I always felt at home. A special thanks to those of you who have had to endure sharing office 32:152 with me. I hope my random outbursts of singing and whistling were not *too* distracting.

I also want to thank the rest of my fellow students of the MENA-program. Not many of us made it through, but you made these five years of studying a pleasant journey, filled with much laughter, and I am grateful to have gotten to know all of you. Further, I must thank the rest of my friends (four-legged included) who have provided me with much-needed breaks, nutrition, tough love and reality checks during this work.

Finally; to my parents. The value of your everlasting support and encouragement cannot be described in words. Thank you!

—***Morten Østigård***, 15.05.19, Oslo.

Contents

List of Figures

List of Tables

Abbreviations & Acronyms

BESS battery energy storage system

BMS battery management system

DOD depth of discharge

EOL end of life

EV electric vehicle

LFP lithium iron phosphate

Li-ion lithium-ion

LIB lithium-ion batteries

LTO lithium titanate

MH metal hydride

NCA lithium nickel cobalt aluminum oxide

NiCd nickel–cadmium

NiMH nickel-metal hydride

NMC lithium nickel manganese cobalt oxide

REE rare earth elements

RES renewable energy source

SEI solid-electrolyte interface

SOC state of charge

1 Introduction

The power system, as we know it, is undergoing significant disruption. Instead of a centralised infrastructure based on large energy producers powered by fossil fuels, distributed renewable energy sources are gaining considerable traction. Until now, the cost of renewable energy sources has been an essential reason for their low degree of penetration. However, with prices plummeting, it is estimated that energy production from solar resources will be responsible for 40% of the global electricity production by 2050, and the same estimate for wind is roughly 29% [1]. This rapid increase is necessary as global energy demand is ever increasing, and is expected to nearly double by 2050 [2]. It is also essential because fossil fuels cannot cover the increase in energy consumption if the world is to meet its targets from the 2015 Paris climate agreement (COP 21).

The rapid increase in renewable energy does not come without challenges. As a consequence of their intermittent and variable nature, renewable energy sources (RESs), such as solar and wind, present stability and reliability issues of power production. The problem will only increase as these energy sources gain penetration into the grid. To help alleviate this problem, solutions which consider energy storage must be introduced to provide a stable and reliable energy supply [3]. Energy storage can help to meet peak electrical load demands, provide time-varying energy management, reduce the influence of intermittent power generation and improve power quality. Not only can energy storage help stabilise the power supply, but it can also be used to electrify off-grid areas in combination with RESs. In 2016, off-grid renewable energy systems served 133 million people, with the market growing six-fold since 2011 [4].

1.1 Challenges

It is evident that the need for renewable energy storage solutions will continue to increase rapidly as RESs gain traction. However, not all energy storage was created equal. Each storage

technology has its characteristics and limitations, making it more or less suitable for a given application. Features of importance are typically response time, storage capacity, and cost. Some storage solutions also have location specific requirements, such as pumped hydro and large-scale compressed air energy storage. In this crowd, batteries stand out as one of the most versatile storage solutions. In general, batteries have short response times, in the range of milliseconds, they are scalable, have high efficiency, are deployable on almost any location; and can deliver both high power and high energy [5].

Another challenge for the power system in coming years is the electrification of the transportation sector. Though the charging of electric vehicles (EVs) often happens at home, availability of public fast-charging stations is of importance for most users at some point. The need for fast charging stations is currently rapidly increasing, and only in Norway, it is estimated that there is a need for around 8000 new fast chargers by 2025; as of January 2019, there were only 1700 stations available [6]. This rapid expansion will be costly as it will require large infrastructure improvements in rural areas, and the charging station provider typically has to pay an investment contribution to cover the expenses which can be of considerable size. Here battery energy storage systems (BESSs) and RESs can be of great help. If off-grid, a BESS can be charged by renewable energy most of the day, and then deliver high surges of power for a shorter amount of time when a car is charging.

Similar to RES, the main drawback of BESSs has been price. For a long time, lead-acid batteries were the most popular alternative for large-scale storage due to their relatively low material cost. With the increasing demand for batteries in consumer electronics, and not at least in EVs, other chemistries have also become viable options. Consequentially, the annual battery energy storage capacity solely for utility-scale application is expected to rise from just 360 MW in 2014 to 14 GW in 2023 [7]. Still, the upfront cost of BESSs is considered high. It is therefore important to have good tools for scientists, engineers and decision makers when considering the feasibility of such systems and to understand how to improve them. Battery models play an important role in this aspect, as they can be used to estimate how a battery system will perform under various conditions and in various scenarios.

Today, renewable energy system simulations, which include batteries, use idealised battery models to keep simulation times at a manageable level and to reduce the overall complexity of the system model. Most often, electrical circuit models are used as they can simulate the electrical behaviour of the battery with high precision. However, this approach does not provide sufficient information and detail when it is necessary to evaluate the long-term performance of the system, as they do not consider performance-reducing effects.

1.2 Motivation and contribution of this thesis

Based on the described challenges, the current models are only partially providing an acceptable description. There is a need to consider more detailed descriptions of battery deterioration, while still being able to simulate within reasonable time limits when integrated into more complex systems. Improved models should take into consideration the following effects: (i) the influence of temperature on the dynamic response, capacity and current-voltage behaviour (ii) the influence of charge/discharge rates on available capacity (iii) the influence of usage (cycling, current, temperature) on battery ageing (iv) the influence of battery ageing on system performance. In this thesis, we make the hypothesis that taking into consideration these parameters will enable more accurate predictions.

To achieve this, we create a semi-empirical battery model of a NiMH battery which combines features from several other models and approaches found in the literature. For example, it takes inspiration from methods used to analyse fatigue data to estimate the effect of cycling stress on the battery system. The model is based, and validated, on real data from industrial providers of BESS.

Further, this work proposes the possibility of powering a non-grid-connected EV charging station, using only renewable energy produced from solar and wind. The system is connected to a BESS to provide stable power output and mitigate the influence of the intermittency and variability of the RES, t which is simulated using the battery model we develop in the first part of the thesis.

Two charging stations with different charging patterns are considered. One that shows seasonal trends, and one which does not. We consider three different scenarios for each station, where we study the feasibility of operating the station using power produced from only solar, only wind, or a combination of the two. We further consider the influence of RES mixture, sizing and charging behaviour. To provide realistic results, we used real data acquired from Norwegian power producers and a Norwegian EV charging operator.

1.3 Organization

This thesis is structured as follows: Chapter 2 introduces relevant theory about electrochemistry, batteries, their limitations and deals in particular with NiMH batteries. Chapter 3 presents information on various approaches for modelling batteries found in the literature,

we develop the battery model used in this thesis, and tests the validity of the model by comparing it to real data. Chapter 4 outlines the details of the system considered in this thesis; we explain the details of the simulation set-up. Further, we present the results and discuss these. Finally, in chapter 5 we summarise our findings and consider some possible directions for future work.

2 Battery theory

The purpose of this chapter is to introduce concepts, definitions and theory used to describe electrochemical cells which will be put to use as we develop our battery model in chapter 3.

2.1 Cell operation principles

A battery can be defined as "one or more electrically connected electrochemical cells having terminals/contacts to supply electrical energy" [8]. A single electrochemical cell consists of two half cells, each of which contains an electrode (electronic conductor) and an electrolyte (ionic conductor, can be both fluid or solid). In contrast to its cousin, the fuel cell, where fuel is supplied externally, and the electrodes are just charge-transfer media; battery electrodes take part in the reaction as active masses. This feature makes it possible for conversion and storage to happen in the same compartment–an essential reason for why batteries have found such a high number of applications.

Electrical energy is generated by conversion of chemically stored energy through reduction and oxidation (redox) reactions happening at the electrode-electrolyte interface. The electrode at which the reduction is happening when the cell is doing electrical work on the environment is called the cathode (+), and the one where oxidation takes place is called the anode (-). Since reactions at the cathode typically take place at a higher potential than the anode, the terms *positive* and *negative* electrodes are commonly used–indicated by plus and minus signs.

We are often interested in knowing how much work a cell can provide under a given set of conditions. For a reversible electrochemical reaction at constant temperature and pressure, the electrical work the cell does on its environment is equal to the change in Gibbs free energy

which again is related to the difference in electrochemical potential of the species involved:

$$w_{elec,rev} = \Delta G = \left(\sum_j \nu_j \mu_j\right) - \left(\sum_i \nu_i \mu_i\right) \tag{2.1}$$

where $\nu_{j,i}$ are the stoichiometric coefficient and $\mu_{j,i}$ are the electrochemical potentials of the product and reactant species respectively. Each electron produce work equal its charge times the potential difference between the electrode. For a reaction involving n electrons under standard-state conditions the amount of work produced per mole is:

$$\Delta G^{\ominus} = -nFE^{\ominus} \tag{2.2}$$

where F is Faraday's number and $E^{\ominus}$ is the cell voltage for the specific chemical composition. Typically a cell might not be operate under standard conditions, but the same relation also holds true under non-standard-state conditions:

$$\Delta G = -nFE \tag{2.3}$$

We see that we need to know the cell potential in order to calculate ΔG. We can calculate this value by the help of the Nernst equation, which is perhaps the most central equation within the field of electrochemistry. To derive this relation we use the fact that the Gibbs free energy of a bulk chemical reaction can be described by the Van't Hoff isotherm:

$$\Delta G = \Delta G^{\ominus} + RT \ln Q \tag{2.4}$$

where Q is the reaction quotient as defined in the law of mass action:

$$Q = \frac{\prod_j a_j^{\nu_j}}{\prod_i a_i^{\nu_i}} \tag{2.5}$$

here $a_{j,i}$ is the activity of the product and reactant species respectively. By combining eqs. (2.2), (2.3) and (2.11) we arrive at the common formulation of the Nernst equation, which relates the eduction potential of a cell or half-cell to the standard-state given the temperature and activities of the species involved:

$$E = E^{\ominus} - \frac{RT}{nF} \ln Q \tag{2.6}$$

We still need to know the standard potential of the cell, but this is often simpler to obtain than the standard Gibbs energy as the standard potential of most common half-cells has been

measured against a standard hydrogen electrode, and is reported in tables. The use of a standard electrode is necessary as we cannot measure the voltage of a half cell alone (we would need two electrodes to conduct the measurement). It can be shown that the total standard potential of the full cell is simply the difference between the standard half-cell potentials: $E^{\ominus}_{total} = E^{\ominus}_{red,1} - E^{\ominus}_{red,2}$. An excerpt from a table over standard reduction potentials can be found in table 2.1.

Table 2.1: Excerpt from standard reduction potential table [9]

Electrode reaction	**Standard Potential $E^{\ominus}$ (V)**
$Li^+(aq) + e^- \rightleftharpoons Li(s)$	-3.04
$K^+(aq) + e^- \rightleftharpoons K(s)$	-2.92
$Ca^{2+}(aq) + 2\,e^- \rightleftharpoons Ca(s)$	-2.76
$Na^+(aq) + e^- \rightleftharpoons Na(s)$	-2.71
$Mg^{2+}(aq) + 2\,e^- \rightleftharpoons Mg(s)$	-2.38
⋮	⋮
$2\,H^+(aq) + 2\,e^- \rightleftharpoons H_2(g)$	0.00
⋮	⋮
$H_2O_2(aq) + 2\,H^+(aq) + 2\,e^- \rightleftharpoons 2\,H_2O(l)$	1.78
$Co^{3+}(aq) + e^- \rightleftharpoons Co_2{}^+(aq)$	1.82
$S_2O_8{}^{2-}(aq) + 2\,e^- \rightleftharpoons 2\,SO_4{}^{2-}(aq)$	2.01
$O_3(g) + 2\,H^+(aq) + 2\,e^- \rightleftharpoons O_2(g) + H_2O(l)$	2.07
$F_2(g) + 2\,e^- \rightleftharpoons 2\,F^-(aq)$	2.87

2.2 Cell limitations

Under ideal conditions, it would be possible to convert all of the energy stored within the electrodes to useful electric energy. However, under real-life conditions, a battery does not operate in its equilibrium state during charge and discharge. Consequently, less energy can be drawn from the battery during discharge, and more energy is needed to charge the battery than one would expect by only taking thermodynamic considerations into account. This deviation is caused by several different kinetic limitations and mechanical side effects, which are collectively referred to as battery polarization. The result is voltage loss, and the conversion of useful energy to waste heat. It is common to quantify polarization in terms of an overpotential, η, which we define as the difference between the cell's operating potential, E', and equilibrium potential, $\eta = E' - E_{eq}$ [10, 11].

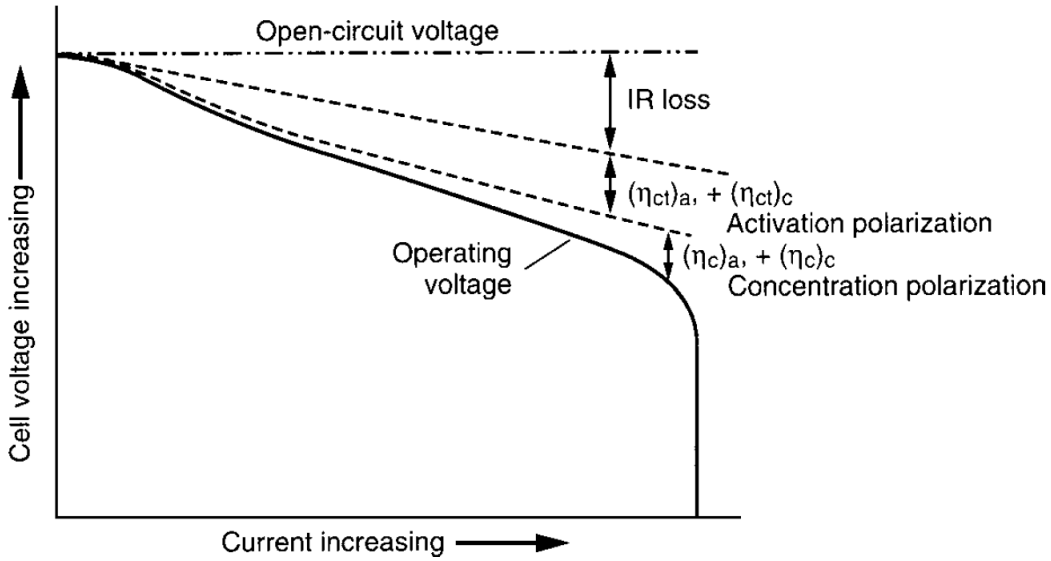

Figure 2.1: Typical polarization curve showing the individual contributions from each type of polarization to the resultant. [11]

As time passes, a battery also delivers lower than expected performance. Battery degradation, or *ageing*, occurs due to unwanted chemical side-reactions. Battery degradation is a complex phenomenon, and each battery ages differently depending on its chemistry, environment and usage. In the following sections, we describe the mechanisms behind polarization and degradation, and their influence on battery performance.

2.2.1 Polarization

Battery polarization is typically divided into three different parts: (i) activation polarization (ii) concentration polarization (iii) ohmic polarization:

$$\eta = \eta_{activation} + \eta_{concentration} + \eta_{ohmic} \tag{2.7}$$

In real-life it might however be challenging to measure the individual contribution to the resultant from each part [8]. Figure 2.1 shows approximately how the battery voltage decreases with increasing current density, and how the individual type of polarization contributes to this decrease. Figure 2.2 illustrates the individual effects on a constant current battery discharge curve.

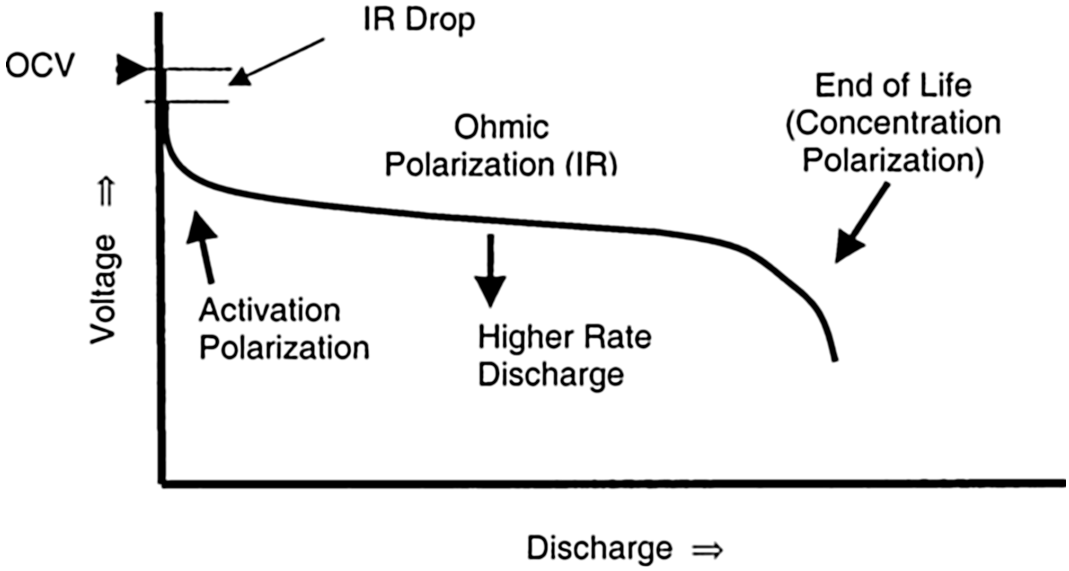

Figure 2.2: Typical discharge curve showing the individual contributions from each type of polarization to the resultant [8]. See glossary for description of the open-circuit voltage

Activation polarization

Electrode reactions can seem straightforward on paper, such as a metal ion being reduced by the transfer of a single electron, $Ox + e^- \longrightarrow Red$, and incorporated into the electrode. However, the mechanism might be complex and involve several reaction steps and limitations. At the electrode-electrolyte interface there exists a Galvani potential difference, $\Delta\varphi = \varphi_M - \varphi_S$, between the bulk electrode, M, and the bulk solution, S. To counteract the potential difference, a double layer of ions with different charge spontaneously arranges on the surface of the electrode as soon as it comes in contact with the electrolyte. Several models with different levels of sophistication have been developed to describe the double layer and the potential difference, which are outside the scope of this work and will not be described here. This double layer causes kinetic limitations to electrochemical red-ox (or charge transfer) reaction(s) taking place at the surface [10].

If a species is to take part in a reaction at this interface, it must migrate through the double layer and adjust its hydration sphere as it discards or receives electrons. The rate at which such an activated process takes place is governed by an activation Gibbs energy, $\Delta^{\ddagger}G$. Activation polarization arises when this becomes the rate-determining step, as energy is needed to drive the process forward [10]. The relation between the rate of reaction happening at the interface and the activation overpotential at the anode and cathode can be related through eq. (2.8),

often referred to as the Butler-Volmer equation after John Alfred Valentine Butler and Max Volmer who first described the relation [12]:

$$j = j_a - j_c = j_0 \left\{ e^{(1-\alpha) n f \eta_{ac}} - e^{-\alpha n f \eta_{ac}} \right\} \tag{2.8}$$

where j_a, j_c, j_0 are the anodic, cathodic and exchange current density in A/m^2 respectively, α is the so-called charge-transfer coefficient ($0 \leq 1$, dimensionless), n is the number of electrons involved in the reaction, $\eta_{ac} = (\eta_{ac})_a + (\eta_{ac})_a$, is the activation overpotential in V and $f = F/RT$ is a purely cosmetic rewrite where F is Faraday's number, R is the ideal gas constant and T is the temperature in Kelvin. In the case where the overpotential is sufficiently small, $f\eta_{ct} \ll 1$, we can simplify the relation by using a power expansion of the exponential terms ($e^x 1 + x$):

$$j = j_0 n f \eta_{ac} \tag{2.9}$$

We see that there is a linear relationship between the current density and the overpotential in this region. We will make use of this relationship in section 3.2.1.

Concentration polarization

In the derivation of the Butler-Volmer equation, one assumes the uniformity of concentration near the electrode surface due to the low conversion of electroactive species at low current densities. At higher current densities, this assumption fails as the consumption of species increases close to the electrode surface—creating a concentration gradient. As current increases, the mass-transport of species from the bulk to the electrode might become the rate-determining step. This effect leads to the need for an increased overpotential to produce a given current [10].

The dominant type of mass-transport in batteries is typically not convection or electrical migration, but the diffusion of species in a concentration gradient to and from the reaction sites to maintain a flow of current. Applying Fick's first law of diffusion and assuming that the thickness of the diffusion layer boundary, is not influenced much by concentration, one can relate the current, i, to the maximum diffusion current, i_L [11]:

$$i = \left(1 - \frac{C_E}{C_B}\right) i_L \tag{2.10}$$

where C_E is the concentration of electroactive species on the electrode surface and C_B is the bulk concentration. Using the Nernst equation the concentration overpotential arising from difference in concentration across the diffusion layer can be written as:

$$\eta_c = \frac{RT}{nF} \ln\left(\frac{C_E}{C_B}\right) \tag{2.11}$$

Rearranging and combining eq. (2.10) and eq. (2.11) we arrive at the following approximation for the concentration overpotential:

$$\eta_c = \frac{RT}{nF} \ln\left(\frac{i_L}{i_L - i}\right) \tag{2.12}$$

According to eq. (2.12) one would expect the overpotential to increase to infinity as i approaches i_L: $\lim_{i \to i_L} \eta_c = \infty$. However, in real life, it will only increase until another reaction occurs [11]. Concentration polarization effects are relatively slow to kick in, with build-up and decay taking ($\geq 10^{-2}$ s) to appear [8].

Ohmic polarization

The third major source of performance loss arises from internal impedance in the battery and is referred to as *ohmic polarization*. As indicated by the name, it behaves according to Ohm's law, meaning it is proportional to the battery current. Ohmic polarization can roughly be divided into two parts: (i) ionic resistance (ii) electrical resistance. Ionic resistance stems from resistance to the flow of ions in the electrolyte, separator and porous electrodes. Electrical resistance stems from the intrinsic resistance to charge flow in battery components, such as the electrodes, current collector and terminals:

$$\eta_{ohmic} = iR_{ohmic} = i(R_{ionic} + R_{elec}) \tag{2.13}$$

The value of the internal resistance depends on several factors such as battery size, chemical composition, temperature, age and discharge current. In general, the individual contribution from each component is inversely proportional to its specific conductivity and thickness, and inversely proportional to its area. Ohmic polarization appears almost instantaneously ($\leq 10^{-6}$ s) when current flows. This behaviour can be observed on battery discharge curves where the voltage drops from the open-circuit voltage to a lower value as soon as the battery is connected to a load. It is therefore often also referred to as the *IR-drop*.

Polarization summarized

To conclude this section: As a battery is connected to a load, we can approximate the operating voltage as the sum of the theoretical cell voltage and overpotentials across the electrodes, the electrolyte, and ohmic losses from contact resistances:

$$E = E_0 - \left[(\eta_{ac})_a + (\eta_c)_a\right] - \left[(\eta_{ac})_c + (\eta_c)_c\right] - i(R_{ionic} + R_{elec}) = iR \tag{2.14}$$

In theory, one could get a good estimate from eq. (2.14). However, in practice it has proven difficult to obtain the necessary values for the parameters needed to calculate activation and concentration polarization. Partly because of the intricate structures of modern day electrodes, which typically are complex composite bodies with porous structure made of active material, binders, additives and fillers [11].

2.2.2 Rate-capacity effect

The rate-capacity effect describes one of the ways battery polarization can influence battery performance. As shown in fig. 2.3–the capacity a battery can deliver decreases when increasing the discharge rate, which is in accordance with our discussion in section 2.2.1. The relation is also sometimes called the*Peukert's effect* after the German scientist Wilhelm Peukert who first described it empirically for lead-acid batteries. Peukert's law often takes the following form:

$$C_p = I^k t \tag{2.15}$$

where C_p is is the discharge capacity in (A h), I is the discharge current in (A), k is Peukert's coefficient (dimensionless, typically in the range 1-2) and t is the discharge time in hours. This relation considers only constant discharge and does not take into account temperature, nor self-discharge, which become important at low discharge currents. The extent of the rate-capacity effect is dependent on battery chemistry and is more evident in some batteries than others [13].

2.2.3 Degradation/ageing

As soon as a battery leaves the production line, it starts to deteriorate through unwanted chemical side-reactions. These side-reactions occur either as a result of cycling, which re-

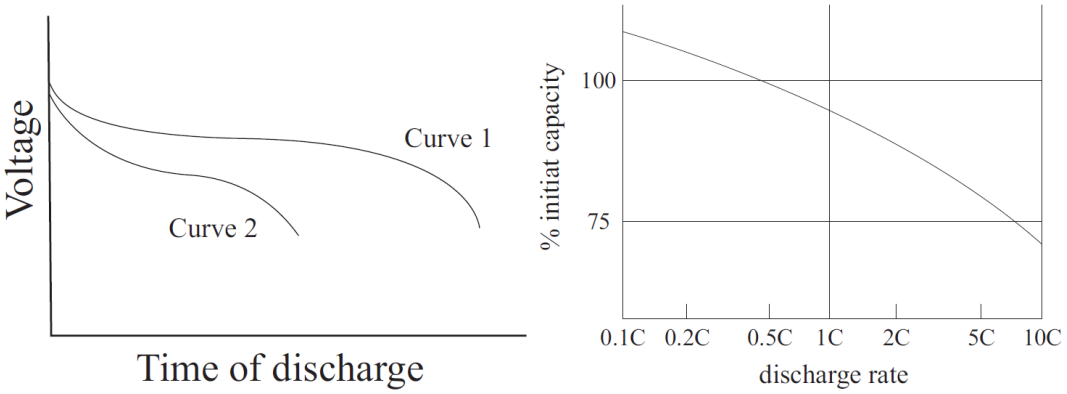

Figure 2.3: Illustration showing the rate-capacity effect. [14]

duces its *cycle life*, or just spontaneously as time passes, which reduces its *calendar life*. The deterioration manifest primarily in three ways:

- Decreased capacity
- Increased internal resistance
- Increased rate of self-discharge

Self-discharge is the decrease in battery capacity without any contact between the electrodes. The phenomenon is more prominent in some chemistries than others but also depends on battery design. For example, the first NiMH batteries could lose as much as 30% of their capacity in the first month, while newer NiMH batteries can lose as little as 30% in 10 years [15]. As a rule of thumb, the rate of self-discharge generally doubles for every 10 °C above nominal temperature for most battery chemistries [11]. Self-discharge is sometimes called *reversible capacity loss*, as it does not lead to a permanent capacity loss in secondary batteries. For primary batteries it is permanent as they cannot be recharged. Consequentially, primary batteries are often labelled with a *shelf-life*, which is the amount of time they can last under certain storage conditions before their capacity fall below a given threshold. With time, the rate of self-discharge in secondary batteries increases.

Different mechanisms might be responsible for irreversible capacity loss, or capacity fade, depending on cell chemistry and operating conditions. Figure 2.4 shows the most important mechanisms leading to capacity fade in NiMH batteries. We see that all of the paths eventually lead to electrolyte dry-out.

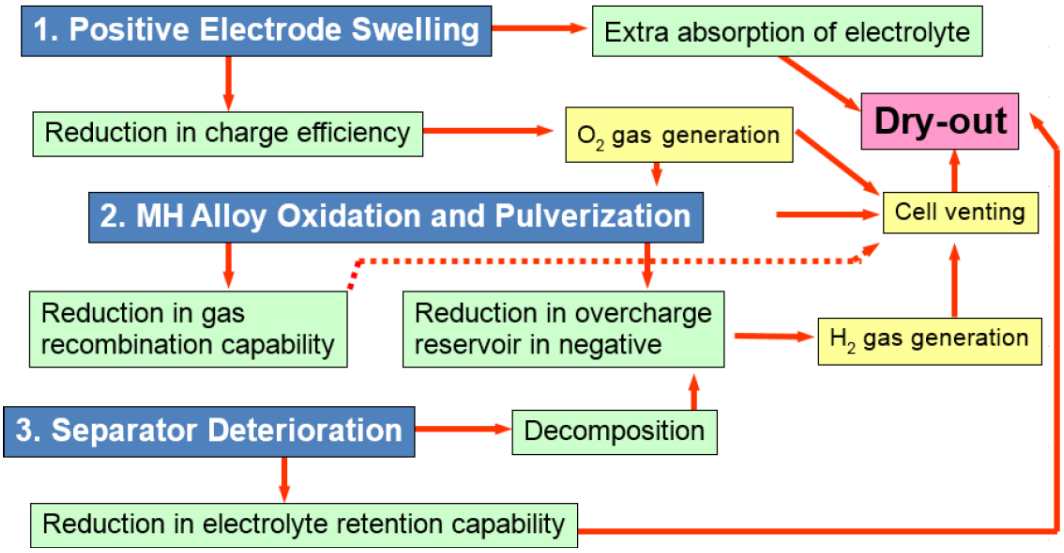

Figure 2.4: Capacity degradation mechanisms in NiMH batteries [16]

2.3 Battery chemistries

In table 2.2 we compare NiMH batteries with lead-acid and lithium-ion (Li-ion) batteries, which are the two most commonly used battery storage technologies for large-scale applications. Some parameters are given as ranges as there can be a large variance in performance within one battery type depending on build, chemistry and design. In particular, we see that Li-ion performance can vary greatly. This is because Li-ion batteries can have various cathode materials such as: lithium nickel cobalt aluminum oxide (NCA), lithium nickel manganese cobalt oxide (NMC), lithium iron phosphate (LFP) and lithium titanate (LTO); each of these have their own strength and weaknesses.

Table 2.2: Comparison of NiMH, lead-acid and Li-ion batteries [11, 17, 18]

Properties	**NiMH**	**Lead-acid**	**Li-ion**
Nominal Voltage (V)	1.2	2.0	3.6
Specific energy (Wh/kg)	70–80	20–50	70–250
Energy density (Wh/L)	170–420	50–100	200–735
Cycle life	500–2000	300–2500	500–20000
Rate capability (C)	a	b	c
Operating temperature (°C)	-30–70	-40–60	-40–65
Cost ($/kWh)	200–400	105–475	200-–1260
Recycled (%)	✓[1]	≥ 95%	≤ 5%

Examining the data, we see that NiMH batteries fall somewhere in-between lead-acid and Li-ion batteries, performance-wise. It becomes evident when looking at the table that one of the compelling arguments against using Li-ion cells is their high cost and that they are barely recycled. While more than 95% of lead-acid batteries are recycled, only 5% of Li-ion batteries are currently recycled globally. This low percentage is tightly linked to the cost of recycling, as recycling the materials is still more expensive than to mine new ones. The rapid development of Li-ion technology also increases the risk of making recycling facilities outdated in only a few years. Additionally, Li-ion batteries have a more complex design and have a wide variety of chemistries compared to NiMH and lead-acid, which makes it more challenging to extract metals during recycling [19–21]. It is, however, reasonable to believe that this can improve as more Li-ion car batteries reach their end of life, technology matures, and raw materials become more expensive.

Li-ion batteries also contain several non-environmentally friendly metals, such as cobalt, copper and nickel, which today end up in landfills. NiMH batteries also contain nickel, cobalt and rare earth elements (REE). However, most of these metals can be recycled, as the NiMH battery is a more mature technology and has proven to be economically viable. Big car companies such as Toyota and Honda, or battery producers such as Nilar AB and Panasonic, all have established contracts or facilities to have their batteries recycled. [19, 22, 23]. As of today, this makes NiMH batteries the greener choice.

2.4 Nickel-metal hydride batteries

The NiMH battery is considered the successor of the Ni – H_2 battery, initially developed for space applications in the 1970s. The Ni – H_2 battery is still used for this application due to its extreme cycle-life, which can reach 40 000 cycles at 40% DOD, and because it can tolerate overcharging and over-discharging (polarity reversal). However, the Ni – H_2 battery has a gaseous H_2 anode, meaning it has a very low energy density (Wh/kg). The NiMH battery has a much higher energy density, as it stores the hydrogen in solid form as a metal hydride [24].

The NiMH battery is also related to the nickel–cadmium (NiCd) battery. They are similar in the way that they both use the redox couple $Ni(OH)_2$/NiOOH as one of the electrodes. Even though the NiCd batteries have some advantageous features, such as remarkable cycle life, impressive fast-charge performance and good performance at lower temperatures, they were

replaced by the NiMH batteries due to cadmium's high toxicity, and today have a very low market share [24].

An appealing argument for using NiMH batteries is safety. NiMH batteries contain water-based, non-flammable electrolyte. For comparison, Li-ion batteries contain a pressurised flammable liquid electrolyte, typically a lithium salt in an organic solvent, which has the potential to be much more hazardous in case of a fault. Li-ion batteries also start to experience electrolyte decomposition above 70 °C. Furthermore, the breakdown of the solid-electrolyte interface (SEI) starts at 80 °C which might lead to thermal runaway [25]. Thermal runaway can propagate heat to other cells, initiating thermal runaway in other cells and other battery packs, causing an extremely dangerous cascade effect [26]. Note that the thermal runaway temperature onset varies with Li-ion chemistry.

In all, NiMH batteries can be considered inherently safer than Li-ion batteries.

2.4.1 Chemistry

The electrochemical reactions at the anode, cathode and for the full cell are as follows, where the forward direction represents charge, and the reverse direction represents discharge:

$$\mathrm{M} + \mathrm{H_2O} + \mathrm{e^-} \rightleftharpoons \mathrm{MH} + \mathrm{OH^-} \qquad (E_0 = 0.490V) \qquad \text{Anode} \tag{2.16}$$

$$\mathrm{Ni(OH)_2} + \mathrm{OH^-} \rightleftharpoons \mathrm{NiOOH} + \mathrm{H_2O} + \mathrm{e^-} \qquad (E_0 = -0.828V) \qquad \text{Cathode} \tag{2.17}$$

$$\mathrm{Ni(OH)_2} + \mathrm{M} \rightleftharpoons \mathrm{NiOOH} + \mathrm{MH} \qquad (E_0 = 1.318V) \qquad \text{Full Cell} \tag{2.18}$$

here M is the hydrogen storage metal/alloy and MH is the respective metal hydride of M. We also show a graphical representation of the whole battery in fig. 2.5. During discharge, Ni^{3+} is reduced to its divalent state, while the metal hydride MH releases hydrogen and is oxidized.

Today the most commonly used cathode materials consist of "co-precipitated spherical hydroxides from Ni, Co, and Zn and some binders, pasted onto Ni-foam via a wet method" [16]. The anode material is typically a REE-based alloy. Traditionally these have been made up of a mischmetal alloy for which $La_{10.5}\,Ce_{4.3}Pr_{0.5}Nd_{1.4}Ni_{60.0}Co_{12.7}Al_{4.7}$ could be a representative composition. These alloys take on an AB_5 type of structure; however, in recent years, REE-based A_2B_7 metal hydrides have gained increased attention and found use in high-energy/low self-discharge applications. The most widely used electrolyte is 30% KOH

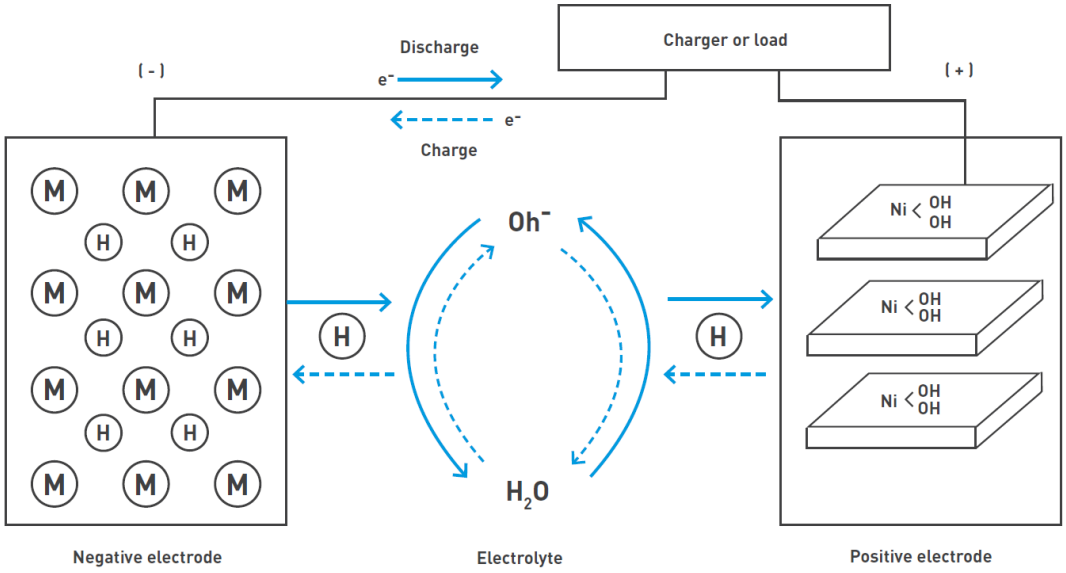

Figure 2.5: Electrochemical operating principle of a NiMH [22]

as it has a good balance between freezing point temperature and conductivity. For high-temperature applications, parts or all of the electrolyte is replaced with less corrosive NaOH. A small amount of more conductive LiOH is sometimes added to boost performance for low-temperature applications [16].

2.4.2 Characteristics & performance

Batteries show different behaviour and performance depending on their chemistry. Below we present original charge- and discharge-curves for NiMH batteries which we also will use to validate our battery model in section 3.7. These curves represent real data provided by the manufacturer, in this case, Nilar AB [22]. We see from fig. 2.6a that the battery performs well, even at higher c-rates. According to the manufacturer's guidelines, the maximum recommended discharge rate is 5C [22]. Figure 2.6b shows how voltage and capacity are influenced by ambient temperature during discharge. We see that although the voltage decreases some with decreasing temperature, the capacity loss is relatively small compared to Li-ion batteries who suffer from low Li diffusion and poor charge transfer at the electrode/electrolyte interface at lower temperatures [27]. The available capacity, of course, depends on the selected discharge cut-off voltage, for this specific battery the manufacturer recommends a cut-off voltage of 1.0V pr. cell [22].

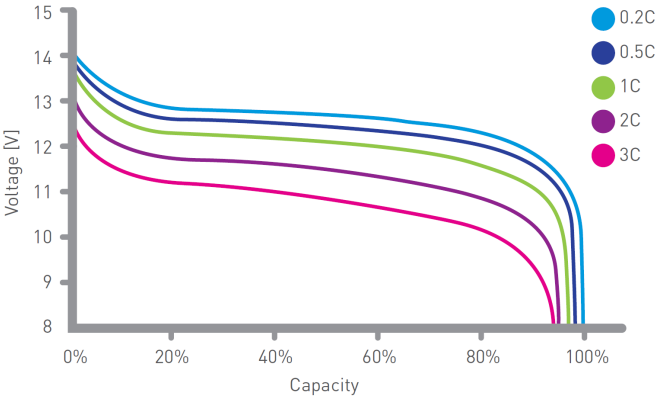

(a) Discharge performance for varying c-rates.

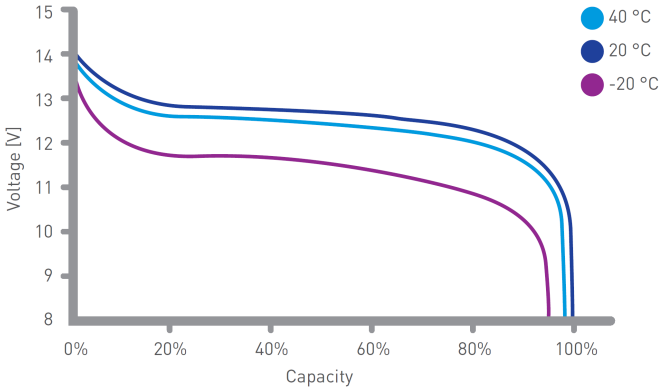

(b) Discharge performance at varying temperatures.

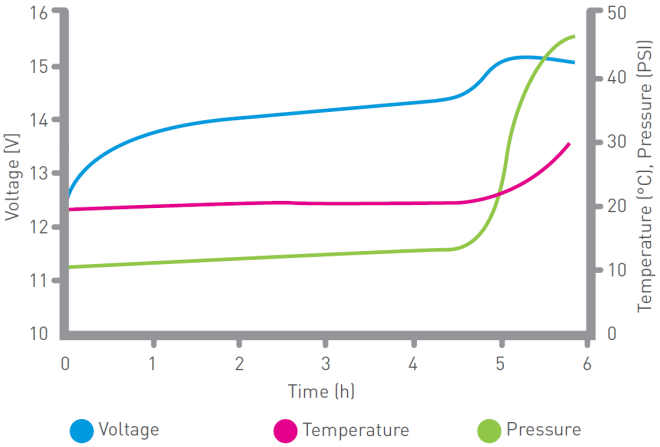

(c) Charging performance.

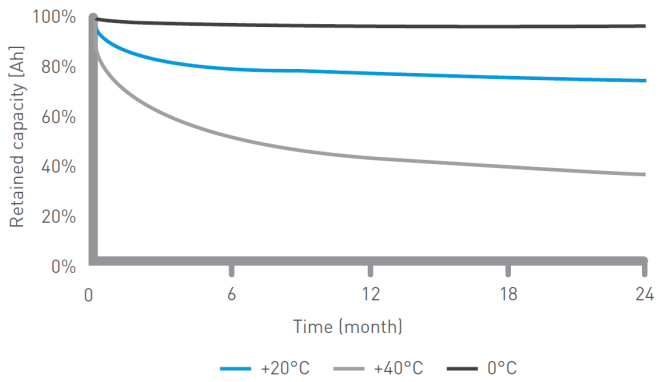

(d) Self-discharge of a fully charged battery.

Figure 2.6: Characteristic NiMH performance curves [22].

Figure 2.6c shows the development of voltage, temperature and internal pressure at 20 °C with a constant current charge rate of 0.2C. We observe that the charging characteristic is very similar to the discharge, except at the end of the charging time. Since the charging process is controlled by a battery management system of which we do not know the specific details, it is difficult to use this information for our model. Only data for one c-rate and one temperature is provided. Finally, fig. 2.6d shows the self-discharge of a fully charged battery at various temperatures. It is evident that most capacity is lost initially, and even at elevated temperatures, the battery retains much of its capacity after two years. The battery manual reports an estimated six % capacity loss after one day and 13 % capacity loss after 28 days for a fully charged pack at 20 °C.

3 Battery modelling: State-of-the-art and model development

In this chapter, we first discuss some popular approaches to battery modelling found in the literature. Further, we describe and develop our model by combining several different methods from the literature with real data. Finally, we check the ability of our model to describe features of interest.

3.1 Battery models: State-of-the-art

Battery systems are highly dynamic and complex systems which have proven difficult to describe accurately. It is, however, of great commercial and scientific interest to be able to describe and predict battery behaviour, as they over time have become an increasingly intrinsic part of our everyday living. Whether they are used in ultra-low-power sensors, for powering an electric vehicle, or for storing renewable energy, accurate and efficient battery models should be part of design and decision-making processes.

As with any modelling problem, there are several approaches which can be taken, not all of which might be fitting for the given problem. In sections 3.1.1 and 3.1.2, we briefly describe the two most common approaches to modelling: 1. electrochemical modelling 2. equivalent circuit modelling. Section 3.1.3 describes the general idea of the approach used in this thesis, which is a semi-empirical model. Note that we in this thesis only have considered models that consider physical quantities, such as current, voltage and temperature, and that is acausal.

3.1.1 Electrochemical modelling

Electrochemical models are by far the most accurate models for describing the complete battery system and what happens in-between the battery electrodes. An electrochemical model tries to represent the actual time- and state-dependent chemical reactions that take place within the battery. Most commonly this is done through a set of partial differential (algebraic) equations, some of which might consider the cell as one-dimensional and others in 2D or even in 3D.

Most of today's physics-based battery models are based on concentrated solution theory to describe the electrolyte, and porous electrode theory to describe the solid phase [28]. This is due to their ability to describe all of the significant chemical interactions and includes essential effects of diffusion and mass transport, temperature-effects and ageing. It would, therefore, be natural to consider these types of models as they can provide the full description.

However, as the fidelity of the model increases, by increasing the number of equations and/or dimension, so does also the computational expense. It is not possible to find algebraic solutions to such a set of equations, and consequentially one has to apply numerical methods to approximate the real solutions. To increase the accuracy of the numeric approximation, one can also decrease the time-steps for which the battery is simulated or increase the spatial resolution, but this too comes at a computational expense.

For this reason, these types of models are not used in system simulations, as simulation times become too large when combined with electrochemical models of other system components. As one of our primary requirements is to develop models which later can be coupled in simulations with other components such as fuel cells, electrolyzers and so on, we did not consider this a good fit for our needs.

3.1.2 Equivalent circuit modelling

In contrast to electrochemical models, which try to describe the electrochemical nature of the battery as truthfully as possible, equivalent circuit models use an abstract representation of the battery which is based solely on electrical components; often as a network of resistors and capacitors. To include non-linear behaviour, one can use diodes, or if high-frequency responses are of interest, one can use resistor-inductor based networks. It can be proven

that by increasing the number of resistor-capacitor components, one can increase accuracy [28].

To configure the models, one relies upon conducting actual measurements of the particular battery, either using electrochemical impedance spectroscopy or by measuring the dynamic response of pulse discharge behaviour. Based on the data, the equivalent circuit network is then fit to the measurements. While this can describe the electrical behaviour of the battery well, it is not possible to tweak parameters of the model if one is interested in looking at the effect of changing one battery feature. This makes this approach rather non-flexible for future use. Additionally, since we in this thesis did not have access to the battery we wanted to model, nor available funding to buy the system, this approach was also considered non-applicable for our needs.

3.1.3 Semi-empirical modelling

The approach towards battery modelling in this thesis is as mentioned what is often described as a semi-empirical approach. This is a general term and indicates that the model is partly based on the underlying principles, and partly relies on the use of empirical data. These types of models are not limited to the battery domain but are used heavily within most fields of science. The motivation for abstracting away is often to reduce computing times, or because a satisfactory description of the system of interest is not possible due to its sheer complexity.

By basing parts of the model on a physical- or chemical description, it makes it possible to tweak parameters that have actual interpretable meaning, and one can thereby study the influence of varying these. That the model is partly empirical and based on empirical data, measurements or observations that one has done means that one can often simulate results with higher accuracy than when considering physics- or chemistry-based models, as there is more information captured in the data.

This hybrid approach provides both flexible combined with efficiency. If the semi-empirical model can be based on data which is typically made available about the system of interest, it makes it also easier to compare various alternatives available. In sum, this motivated the use of this approach in this thesis.

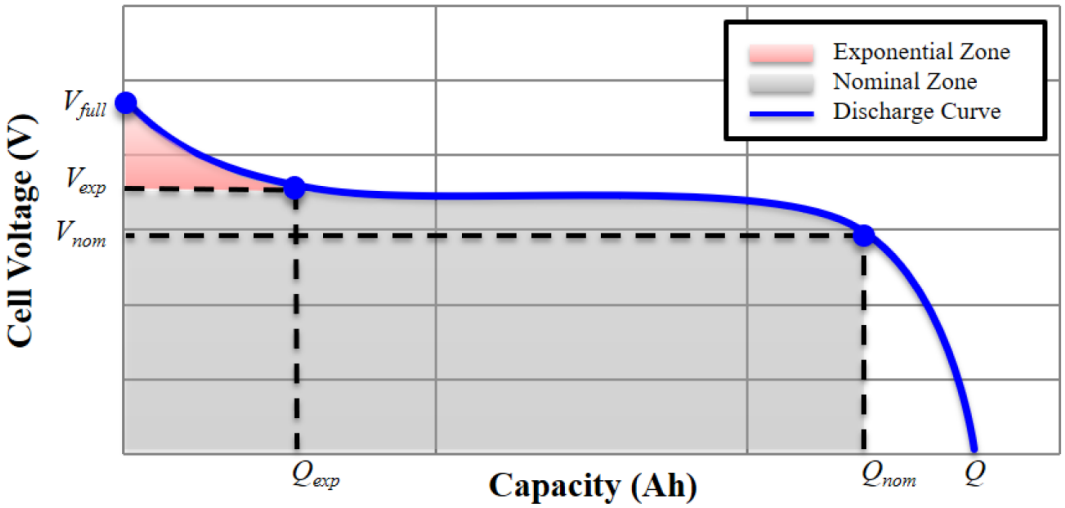

Figure 3.1: General discharge curve showing how a battery discharge can be separated into an exponential zone and a nominal zone [30].

3.2 Voltage model

An essential part of a battery model is to be able to describe its voltage behaviour, which varies depending on a multitude of factors.

3.2.1 Shepherd model

In 1965, C.M. Shepherd published a semi-empirical model to describe the discharge of an electrochemical cell. It was part of a series of papers whose goal was ultimately to design batteries with better properties [29]. The Shepherd-model is based on four assumptions:

1. The anode and cathode have porous active materials.
2. The electrolyte resistance is constant throughout discharge.
3. The cell is discharged at a constant current.
4. The polarization is a linear function of the active material current density.

As a starting point we return to our conclusion from section 2.2.1 where we stated that at low over-potentials the Butler-Volmer equation, eq. (2.8), can be approximated as $j = j_0 nf\eta_{ac}$.

Reversing the relation we get the overpotential which must exist if a current density, j, has been established by an external load:

$$\eta_{ac} = \left(\frac{RT}{nFj_0}\right)j \tag{3.1}$$

If the Butler-Volmer equation is applicable for a cell, this relationship is a good approximation up to $\approx 0.03\mathrm{V}$, but we can get a pretty good fit for the relation with a linear approximation for η_{ac} between $0.02 - 0.04\mathrm{V}$ up to about $0.2 - 0.4\mathrm{V}$. This covers most polarization during normal battery discharge [29]. In fig. 3.1 we show a discharge curve which is divided into two zones: (i) Exponential zone (ii) Nominal zone. In this model, it is assumed the polarization is linear in the nominal zone. If only taking polarization into account, the anodic and cathodic potential during discharge is:

$$V_a = V_{0,a} - K_a j_{am} \qquad \text{Anode} \tag{3.2}$$

$$V_c = V_{0,c} - K_c j_{am} \qquad \text{Cathode} \tag{3.3}$$

where $V_{0,a/c}$ is a constant potential (V), $K_{a,c}$ is the anode/cathode coefficient of polarization (cm^2) and j_{am} is the active material current density ($\mathrm{A/cm}^2$). The use of these equations as the basis for the following derivation does not mean that most battery discharges behave according to the Butler-Volmer equation. It shall prove to be a robust approximation nevertheless. The Shepherd model continues to deal with current density, but for most use-cases it is more practical to deal with current. We will therefore make the switch from current density, j, to current, i, and assume details about the surface geometry to be baked into the constant terms. For a porous electrode, the active material current, i_am, is inversely proportional to the remaining capacity (amount of unused active material):

$$i_{am} = \left(\frac{Q_{a,c}}{Q_{a,c} - it}\right)i \tag{3.4}$$

here $Q_{a,c}$ is the capacity at the respective electrode ($\mathrm{A\,h}$), $it = \int idt$ is the drained battery charge at time t, and i is the discharge current. By combining eqs. (3.2) to (3.4) the expressions become:

$$V_a = V_{0,a} - K_a\left(\frac{Q_a}{Q_a - it}\right)i \qquad \text{Anode} \tag{3.5}$$

$$V_c = V_{0,c} - K_c\left(\frac{Q_c}{Q_c - it}\right)i \qquad \text{Cathode} \tag{3.6}$$

The full cell potential is $V_{\text{batt}} = V_a + V_c$. By assuming that the anodic and cathodic capacity is equal in a well-designed battery cell, $Q_a = Q_c = Q$, and combining eqs. (3.2) and (3.3) the full cell potential can be written as:

$$V_{\text{batt}} = V_0 - K\left(\frac{Q}{Q - it}\right)i \tag{3.7}$$

where $V_0 = V_{0,a} + V_{0,c}$ and $K = K_a + K_c$. When also taking the internal resistance, R, into account the full Shepherd-model becomes:

$$V_{\text{batt}} = V_0 - K\left(\frac{Q}{Q - it}\right)i - Ri \tag{3.8}$$

This equation does not describe the initial potential drop when connecting a battery to a load, but Shepherd includes this in by adding an exponential term has been shown to describe the initial drop with high accuracy in almost every case [29]:

$$A_0 e^{-(B/Q)\cdot it} \tag{3.9}$$

where A_0, B are empirical constants which can be fit to discharge data. The full Shepherd-model is then:

$$V_{\text{batt}} = V_0 - K\left(\frac{Q}{Q - it}\right)i - Ri + Ae^{-(B/Q)\cdot it} \tag{3.10}$$

The Shepherd model is a simple, but effective model for describing battery voltage independent of battery chemistry without involving partial differential equations. However, it has some obvious flaws. It does not does not take into account the rate-capacity effect as we described in section 2.2.2. It does not consider the influence of temperature, nor self-discharge. It also does not deal with degradation.

3.2.2 Modified shepherd model

An improved model was published by Song *et al.*, which addresses several of these concerns. Starting from eq. (3.10) the capacity, Q, is modified to be a function of current:

$$V_{\text{batt}}(t) = V_0 - K\frac{Q(i)}{Q(i) - it} - Ri + Ae^{-(B/Q)\cdot it} \tag{3.11}$$

where the capacity, $Q(i)$, is defined as the following:

$$Q(i) = \left(\frac{i}{i_0}\right)^{\alpha} Q_0 \tag{3.12}$$

which is a reformulation of Peukert's law as described in section 2.2.2 [32]. Here i_0 is the nominal/*reference* current (A), Q_0 is the nominal/*reference* capacity and α is a constant which can be related to the Peukert coefficient ($\alpha = (k-1)/(2-k)$)[32]. Extending the model to take into account variations in voltage with cycle-number (age) and temperature:

$$V_{\text{batt}}(t, i, n, t_r(n), T) = V(n,T) - R(n,T)i - K(n,T)\frac{Q(i,n,T)}{Q(i,n,T) - it} + A(n,T)e^{-(B/Q)\cdot it} \tag{3.13}$$

In the paper by Song *et al.*, the constants were approximated as linear functions of cycle number, n, and temperature, T. From the data in section 2.4.2, we see however that the temperature dependency has a quadratic character. We therefore modify as follows:

$$V(n,T) = V_0(1 + k_{Vn_1}(n-1)) \times \left(1 + k_{VT_2}(T - T_{\text{ref}})^2\right) \tag{3.14}$$

$$R(n,T) = R_0(1 + k_{Rn_1}(n-1)) \times \left(1 + k_{RT_2}(T - T_{\text{ref}})^2\right) \tag{3.15}$$

$$K(n,T) = K_0(1 + k_{Kn_1}(n-1)) \times \left(1 + k_{KT_2}(T - T_{\text{ref}})^2\right) \tag{3.16}$$

$$A(n,T) = A_0(1 + k_{An_1}(n-1)) \times \left(1 + k_{AT_2}(T - T_{\text{ref}})^2\right) \tag{3.17}$$

where k_{Xn_1} is the first-order degradation rate constant related to cycling for parameter X, k_{XT_2} is the second-order degradation rate constant related to temperature and T_{ref} is a reference temperature. A similar modification can be made for the capacity-term with regards to temperature:

$$Q(i,T) = Q_0\left(\frac{i}{i_0}\right)^{\alpha}\left(1 + k_{QT_1}(T - T_{\text{ref}}) + k_{QT_2}(T - T_{\text{ref}})^2\right) \tag{3.18}$$

However, we save the adjustments regarding cycle-number for a more detailed discussion.

3.3 Ageing model

The variable that keeps track of battery age in our model is the number of battery discharge-charge cycles, n. This is useful as most battery manuals specify a cycle-life for the battery. Specifically, the battery's cycle-life is defined as the number of charge-discharge cycles a battery is expected to deliver (cycling under a specific set of conditions) before it reaches its end of life. The cycle-life is dependent on many factors, including [33]:

- Temperature during charge and discharge

- Charge and discharge current
- Depth of discharge
- Method of charge control
- Exposure to overcharging and over-discharging
- Storage conditions

The most important factors to control are depth-of-discharge, temperature and c-rate. We, therefore, describe the influence of each of these parameters in the following sections and how we try to incorporate them into our model.

3.3.1 Depth of discharge

Often, cycle-life is reported for full cycles to 100% depth-of-discharge, or in some cases for a different percentage depending on the application. However, in newer battery manuals it has become custom to report the relationship between cycle-life and depth-of-discharge for the entire range of discharge depths from 0-100%. Figure 3.2 shows this relationship for a NiMH cell from Nilar AB. We observe that the number of cycles to failure has a seemingly inverse exponential relationship to depth-of-discharge. This implies if converted into amp hours, a battery will deliver more charge throughout its life if cycled to a lower depth-of-discharge.

Here we must point out that there exist several definitions of depth-of-discharge. It is most often defined as the inverse of the state-of-charge, meaning a 25% SOC is equal to a 75% DOD. However, it is also commonly used to represent the percentage-wise change in SOC from its previous state. According to this definition, discharging a battery from 75% to 25% SOC is equal to a 50% DOD. For clarity, we will refer to this as *relative* DOD. Looking at fig. 3.2, it is tempting to assume that cycle-life is reported for relative DOD. This is however not the case, as literature confirms that Li-ion batteries cycled at different ranges, e.g. between 25-75% and 50-100%, age at (slightly) different rates [34]. These types of measurements are seldom conducted, and we have not seen it reported in battery manuals. To the best of our knowledge, there are a complete lack of this type of data for NiMH batteries. We, therefore, have to accept the approximation that cells age the same when cycling at the same relative DOD in the following discussion.

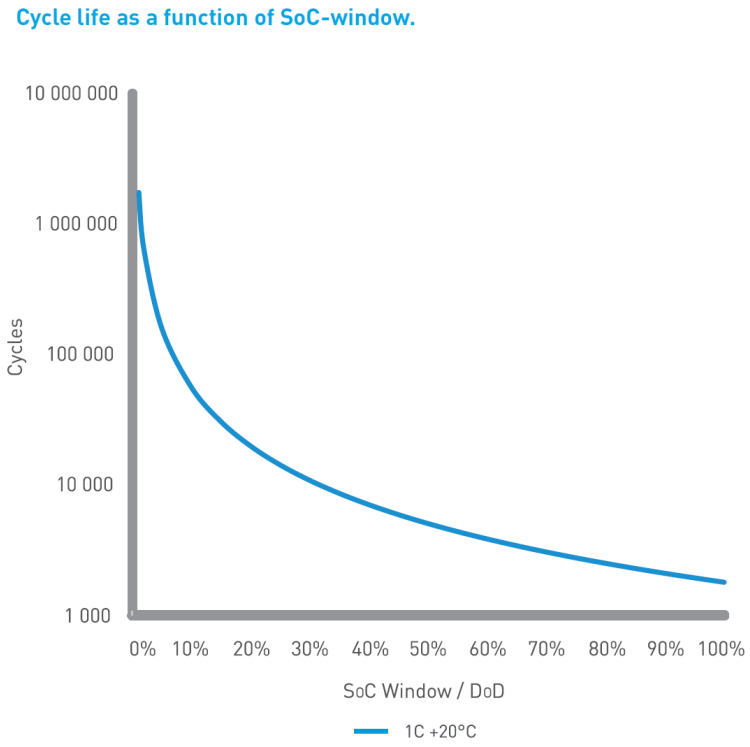

Figure 3.2: Cycle-life as function of depth-of-discharge for a NiMH cell delivered by Nilar AB [22].

Another challenge is that cycle-life is only meaningful when the cycle pattern is regular. However, when a battery is connected to one or more RESs, the result is a current-history consisting of irregular, overlapping cycles, and half-cycles. For some applications with semi-regular cycling patterns, like EVs, there are sometimes developed one or more standardised cycles for battery testing that are considered to represent "normal" use [35]. However, renewable energy is inherently fluctuating, intermittent, and set-ups and conditions can vary greatly. This is probably the reason why standardised cycling patterns have not been developed, at least to the best of our knowledge. Also, standard battery manuals report nothing else than regular discharge-charge cycles, so by some means, we must the cycling history (our simulation data) into an estimated number of *equivalent* full cycles.

One approach to this would be simply to count the amp-hours through current integration. However, this would overestimate the number of full cycles greatly as we have already mentioned. Instead, we propose the use of a cycle-counting algorithm, specifically a *rainflow-counting algorithm*. This algorithm was originally developed for fatigue analysis [36] but has been successfully used to calculate battery degradation[37]. It works by first reducing a variable stress history to a set of constant amplitude events, and after that, it combines smaller

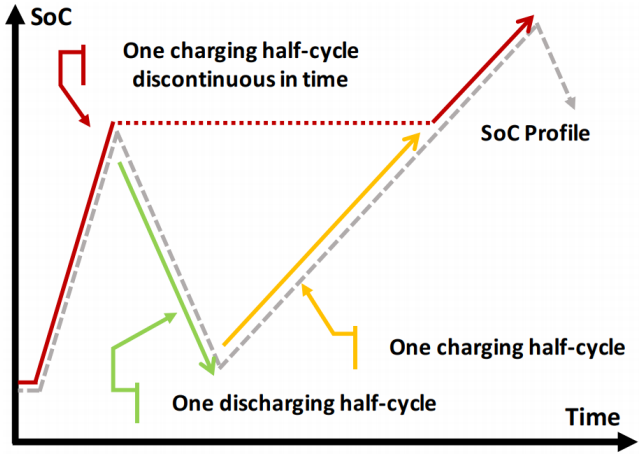

Figure 3.3: Minimal rainflow-counting example. The green and yellow half-cycles can be combined into one full cycle. The red part can be combined into one half-cycle that is discontinuous in time. [37]

discharge-cycles, which can be separated in time, into larger discharge cycles. Figure 3.3 shows visually what this looks like and the algorithm is outlined in algorithm 1. To calculate the influence of each discharge cycle returned by the rainflow-counting algorithm, we must describe the relationship between the cycle-life and depth-of-discharge. We can fit the data by the following expression [38]:

$$1/N = C \cdot D^{\beta} \tag{3.19}$$

where N is the number of cycles, D is the depth-of-discharge given as fraction between (0-1), and C, β are fitted constants. Here C is scaled so the degradation reaches 0.2 (or a different value if specified) at end of life. Figure 3.4 shows the fit to the cycle-life from Nilar AB. From algorithm 1 we obtain the number of discrete cycles for each depth-of-discharge. Using eq. (3.19), the fraction of degradation from each cycle is calculated and summed to obtain the total degradation:

$$D_{cyc} = \sum_{i=0}^{N} C \cdot D_i^{\beta} \tag{3.20}$$

where D_i is the depth-of-discharge of each cycle.

3.3.2 C-rate and temperature

The two other prominent variables that accelerate ageing are charge/discharge-rate and temperature. The effect of each parameter is unfortunately notoriously difficult to separate since

Algorithm 1: Rainflow count algorithm as described by Shi *et al.* [37].

Data: SOC history
Result: cycle count for each relative DOD

1 reduce SOC history to sequence of extrema;
2 count the path between the global maximum and minimum as one half cycle;
3 **if** *global maximum occurs first* **then**
  a. Count as half-cycles: The path between the global maximum and the most negative minimum occurs before it, the most positive maximum occurring before this minimum, and so on to the beginning of the history;
  b. Count as half-cycles: The path between the global minimum in the history and terminate at the most positive maximum occurring subsequently, the most negative minimum occurring after this maximum, and so on to the end of the history;
else
  In the case where the global minimum occurs first, adjust step 3a, 3b accordingly to pair up sequential most positive maximum and most negative minimum that happen before the global minimum, or after the global maximum;
end
4 Count the remaining cycles as small **full cycles**;

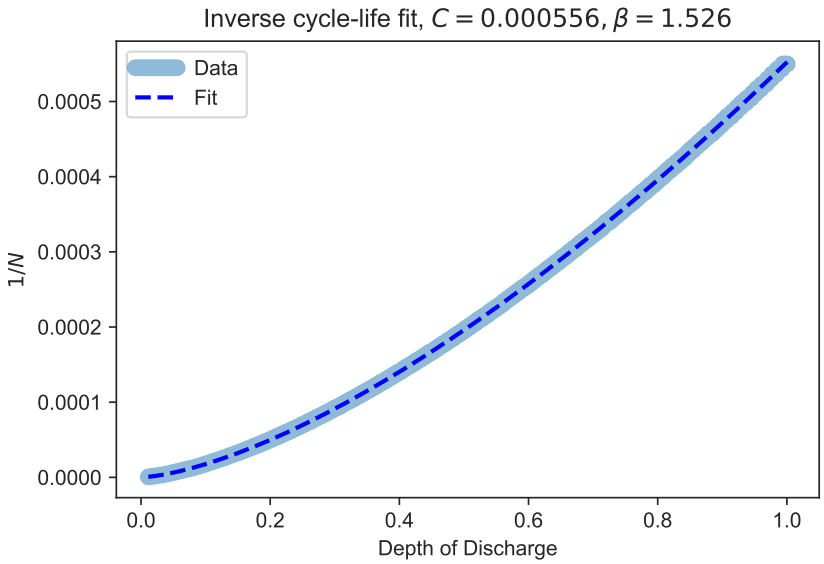

Figure 3.4: Fit of inverse cycle-life as function of DOD(0-1).

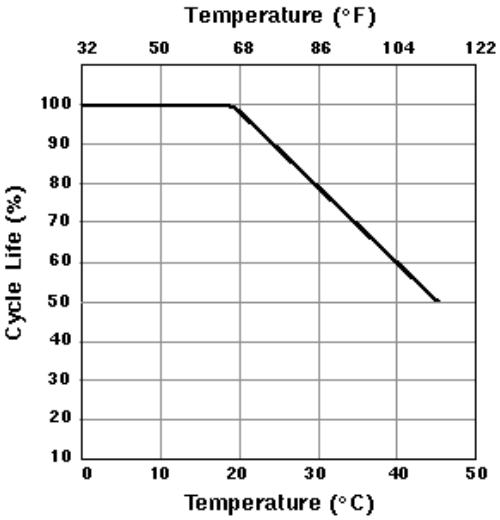

Figure 3.5: Cycle-life as function of ambient temperature [33]. Battery cycled at C/4 charge/discharge rate. Capacity measured at room temperature.

charging and discharging the battery increases the internal temperature of the cell. The combined effect is most likely higher during battery ageing experiments as batteries are typically cycled continuously to save time. Consequentially, they are likely to be subjected to a higher average temperature and faster ageing than they would, given a more normal usage-pattern at room temperature over that given period.

However, if the battery is subjected to high *ambient* temperatures during normal use, cycle-life might be much shorter than expected based on accelerated cycling tests, as ”accelerated” cycle testing does not consider cell ageing with calendar life, which is highly dependant on temperature. Figure 3.5 shows the influence of ambient temperature on cycle-life.

It has proven difficult to obtain high-quality data for the influence of temperature and c-rate on the ageing of NiMH batteries. For Li-ion batteries, some cathode materials are more commonly found in commercial batteries, as mentioned in section 2.3, than others. With the increased popularity of Li-ion, this has motivated researchers to conduct more detailed cycling experiments and to publish complete sets of cycling data, considering the influence of, e.g. varying temperatures and c-rates [39, 40]. For NiMH batteries this is not the case. The chemical variation in anode materials is much more considerable, and each manufacturer has typically patented the anode material of their battery. Consequentially, one is dependant on the companies releasing detailed data themselves, which is unlikely, or for researchers to perform ageing experiments, which is also questionable as it might not be very applicable for developing life-prediction models for other NiMH batteries.

Still, it is of interest to approximate the influence of these parameters in our model. To do this, we consider a lumped temperature model for the internal temperature of a battery, which is a function of current and ambient temperature. We after that, find the average temperature the battery is subject during the simulation and reduce the cycle-life of our battery following fig. 3.5. In this way, we indirectly consider the influence of c-rate, as batteries heat quickly during rapid discharge and charge. High currents can facilitate other side-reactions than high-temperatures, but following our discussion from the beginning of this subsection, the combined effect is difficult to separate.

Temperature model

As we have already discussed, during charge and discharge some energy is lost as heat– increasing the internal temperature. For this reason, and to prevent thermal runaway, larger battery packs typically have some external cooling system. The type of cooling will depend on the application and battery requirements.

If there exists a temperature gradient, heat can be transferred in three ways: (i) Conduction (ii) Convection (iii) Radiation. Often all of these effects can be at play, but depending on the type of cooling, one might be dominant. Due to this combination, heat transfer can be very complex to model precisely, especially when convection must be taken into account as it is described by fluid mechanics. Heat distribution within the battery is also typically not uniform, and much effort can be spent into developing good spacial models for thermal management and when designing cells. However, since the spatial thermal distribution is not the focus of this thesis, we will assume uniform temperature distribution in this thesis. We start by assuming that heat generation arises only from internal resistance. This assumption is not completely true as heat is also generated/consumed due to reversible entropy change resulting from cell electrochemical reactions, but this effect is small at reasonable usage rates [41] and can be neglected. The heat generated is then:

$$\dot{Q} = I^2 R \tag{3.21}$$

where I is the charge or discharge current (A), and R the internal resistance (Ω). The energy balance depends on the heat generated and the heat transfer from the battery to ambient. We assume that the battery pack to be placed in a temperature regulated space which holds constant temperature and that conduction and radiation are the dominant effects. We also assume a lumped thermal capacity, that temperature is evenly distributed in the

battery, and simplify the heat transfer by considering heat transfer to be governed by an overall heat transfer coefficient between battery surface and its surrounding fluid h (W/K):

$$\dot{Q} - (T - T_a)h = mc\dot{T} \tag{3.22}$$

where T is the battery temperature (K), T_a is ambient temperature (K), m is the battery mass (kg) and c is the weighted-average module heat capacity (J/(kgK)). This differential equation can be solved analytically and has the following explicit solution [38]:

$$T_{i+1} = \left(T_i - T_a - \frac{\dot{Q}}{h}\right)\exp\left(-\frac{h}{mc}\,\mathrm{d}t\right) + \frac{\dot{Q}}{h} + T_a \tag{3.23}$$

where T_i is the temperature at time i, and T_{i+1} is the temperature after one time-step. From the temperature-log we calculate the current average temperature, T_{avg}. We then reduce the cycle life according to fig. 3.5:

$$D_{temp} = \begin{cases} 1 & T \leq 20\,^{\circ}\mathrm{C} \\ 1 + (T_{avg} - 20) \cdot k_{TD_1} & T > 20\,^{\circ}\mathrm{C} \end{cases} \tag{3.24}$$

where $T_{TD_1} = -0.02$ is the derivative of the slope in fig. 3.5.

3.3.3 Capacity model

We now modify the capacity model as follows:

$$Q(i, n, T) = Q(i, T) \cdot \overbrace{\tilde{Q}(n, T_{avg}))}^{\text{degradation}},\ n = 1, 2, \ldots \tag{3.25}$$

where $\tilde{Q}$ is defined as:

$$\tilde{Q} = (1 - D_{cycle}/D_{temp}) \tag{3.26}$$

Although in reality, the cycle life is reduced, the model depends on the number of cycles to be the same. We, therefore, calculate the equivalent cycle number as follows:

$$n = 1 + \left(\frac{D_{cycle}/D_{temp}}{C \cdot 1^{\beta}}\right) \tag{3.27}$$

The influence of temperature on the model is therefore not a decrease in cycle-life, but a more rapid increase in cycle life than at lower temperatures. For the calculations this has no real influence. Finally, the complete capacity model can then be written as:

$$Q(i,n,T) = Q_0\left(\frac{i}{i_0}\right)^{\alpha} \times \left(1 + k_{QT_1}(T - T_{\text{ref}}) + k_{QT_2}(T - T_{\text{ref}})^2\right) \times (1 - D_{cycle}/D_{temp}) \quad (3.28)$$

3.4 Parameter estimation

To estimate the parameters for the model, the following data is needed:

- Discharge data for two different discharge currents, i_1, i_2.
- Discharge data at two different ambient temperatures, T_1, T_2
- Discharge data at two different cycle numbers, n_1, n_2
- The relationship between depth-of-discharge and cycle-life
- The relationship between ambient temperature and cycle-life

The data was extracted by using im2graph, a free-to-use digitizing software for converting graphs and plots to data. In cases where the graphs did not show the intercept with the x- and y-axis clearly, the graph was extrapolated using a suitable function using the curve fitting tool in MATLAB.

To estimate the parameters V_0, R_0, K_0, A_0, B and m, one can use the method explained by Tremblay *et al.* [42]. Given discharge data for two different discharge currents $i_1 > i_2$, and the value for the nominal capacity, Q_0, which is specified in most battery manuals; one can select a subset of points along the discharge curves and construct a set of equations to find the best fit for these parameters. The points, $P_1(V_1, Q_1) \ldots P_5(V_5, Q_5)$ must fulfil the following requirements on the $i = i_1$-curve: (i) $P_1(V_1, 0)$ is to be set at beginning of discharge curve (ii) $P_2(V_3, Q_3)$, $P_3(V_3, Q_3)$ must be within the exponential area and fulfil the requirement $Q_3 = 2Q_2$ (iii) $P_4(V_4, Q_4)$ should be set near the end of the nominal zone (iv) $P_5(V_5, Q_5)$ is to set at the end of discharge. P_6 should be within the nominal zone for a different discharge current, $i = i_2$. Figure 3.6 shows these points for the Nilar EC NiMH battery used in this thesis. The following set of equations are used to determine the parameters, for the full derivation the reader is referred to the original paper.

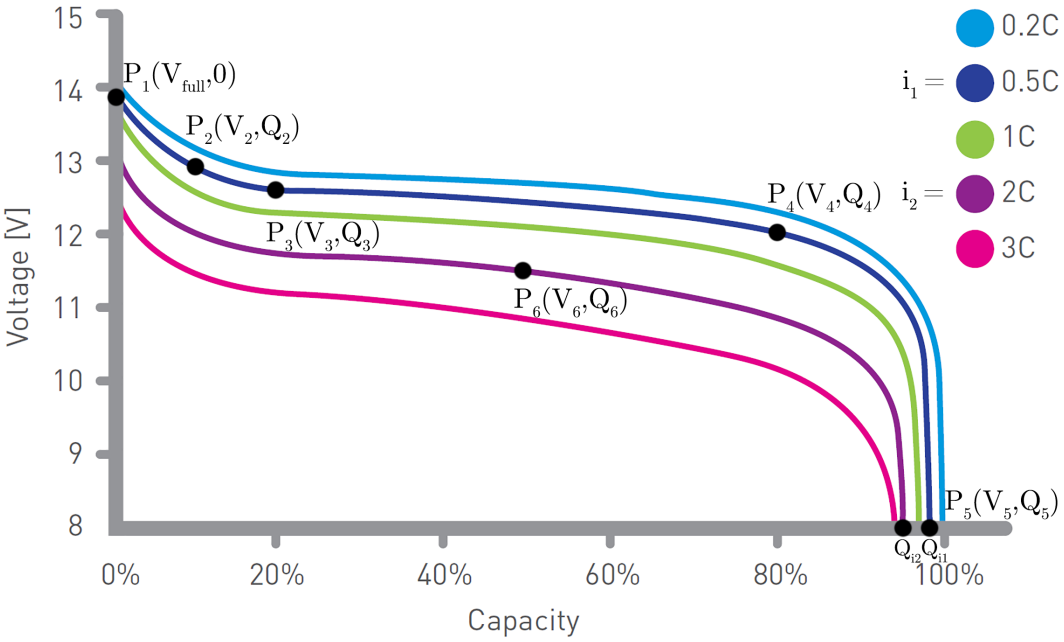

Figure 3.6: Selected points for discharge data at different c-rates used in this thesis.

$$B = -\frac{1}{Q_2}\ln\left(\frac{V_1 - V_3}{V_1 - V_2} - 1\right) \tag{3.29}$$

$$A = \frac{V_1 - V_3}{1 - \exp(-BQ_3)} \tag{3.30}$$

$$s_1 = K\left[\frac{mQ_{i_1}}{mQ_{i_1} - Q_4} - 1\right] s_2 = K\left[\frac{mQ_{i_1}}{mQ_{i_1} - Q_5} - 1\right] \tag{3.31}$$

$$m = \frac{1 - \frac{s_2}{s_1}}{1 - \frac{s_2}{s_1}\frac{Q_4}{Q_5}} \times \frac{Q_4}{Q_{i_1}} \tag{3.32}$$

$$K = s_2\left[m\frac{Q_{i_1}}{Q_5} - 1\right] \tag{3.33}$$

$$R = \frac{1}{i_1 - i_2}\left\{V_6 + K\frac{mQ_{i_2}}{mQ_{i_2} - Q_6} + A\exp(-BQ_6) - \left[V_3 + K\frac{mQ_{i_1}}{mQ_{i_1} - Q_3} + A\exp(-BQ_3)\right]\right\} \tag{3.34}$$

$$V_0 = V_1 + Ri_1 + K - A \tag{3.35}$$

To estimate the first-order constants related to cycle number, k_{Vn_1}, k_{Rn_1}, k_{Kn_1}, k_{An_1} one needs discharge data for two cycle numbers, $n_2 > n_1 > 1$, for the same discharge current i_n and at the reference temperature, T_{ref}. The points $P_7(V_7, Q_7) \ldots P_9(V_9, Q_9)$ should fulfil the following requirements on the $i = n_2$-curve: (i) $P_7(V_7, 0)$ is to be set at the beginning of discharge curve (ii) $P_8(V_8, Q_8)$ should be set within the nominal area (iii) $P_9(V_9, Q_9)$ is to be set at the end of discharge. Such data was not provided by Nilar AB [22]. However, a paper published by Shen *et al.* [24] contained cycling data for the battery in question. The resistance, mid-voltage and capacity after 1380 cycles at a discharge rate of 0.9C and $T = 20\,^{\circ}\text{C}$ was reported. From this data, we can estimate the needed points. To determine the parameters, we solve the following system of equations, here formulated as a matrix equation. Again, the reader is referred to the original paper for the derivation.

$$\boldsymbol{k}_{\text{Xn}} = \boldsymbol{G}^{-1}\boldsymbol{b} \tag{3.36}$$

$$\boldsymbol{k}_{\text{Xn}} = \begin{pmatrix} k_{Vn_1} \\ k_{Rn_1} \\ k_{Kn_1} \\ k_{An_1} \end{pmatrix}; \; \boldsymbol{b} = \begin{pmatrix} V_1 - (V_0 - R_0 i_1 - K_0 + A_0) \\ V_7 - (V_0 - R_0 i_n - K_0 + A_0) \\ V_8 - \left(V_0 R_0 i_n - K_0 \dfrac{mQ}{mQ - Q_8} + A_0 \exp(-BQ_8) \right) \\ V_9 - \left(V_0 R_0 i_n - K_0 \dfrac{mQ}{mQ - Q_9} + A_0 \exp(-BQ_9) \right) \end{pmatrix} \tag{3.37}$$

$$\boldsymbol{G} = \begin{pmatrix} V_0 & -R_0 i_1 & -K_0 & A_0 \\ V_0(n_2 - 1) & -R_0 i_n (n_2 - 1) & -K_0(n_2 - 1) & A_0(n_2 - 1) \\ V_0(n_2 - 1) & -R_0 i_n (n_2 - 1) & -K_0(n_2 - 1)\dfrac{mQ}{mQ - Q_8} & A_0(n_2 - 1)\exp(-BQ_8) \\ V_0(n_2 - 1) & -R_0 i_n (n_2 - 1) & -K_0(n_2 - 1)\dfrac{mQ}{mQ - Q_9} & A_0(n_2 - 1)\exp(-BQ_9) \end{pmatrix} \tag{3.38}$$

where the capacity Q is the capacity at $T = T_{\text{ref}}$, $i = i_n$ and $n = n_2$. Song *et al.* suggests that the internal resistance increase is neglectable within a certain life-span. This is in accordance with the measurements conducted by Shen *et al.*, and so the internal resistance deviation with respect to cycle-number is modified as follows:

$$k_{Rn_1} = \begin{cases} 0, & n \leq n_0 \\ k_{Rn_1} & n > n_0 \end{cases} \tag{3.39}$$

Finally, to estimate the second-order temperature constants. k_{VT_2}, k_{RT_2}, k_{KT_2}, k_{AT_2} one needs discharge information for two different temperatures, T_1, T_2, at the same discharge current

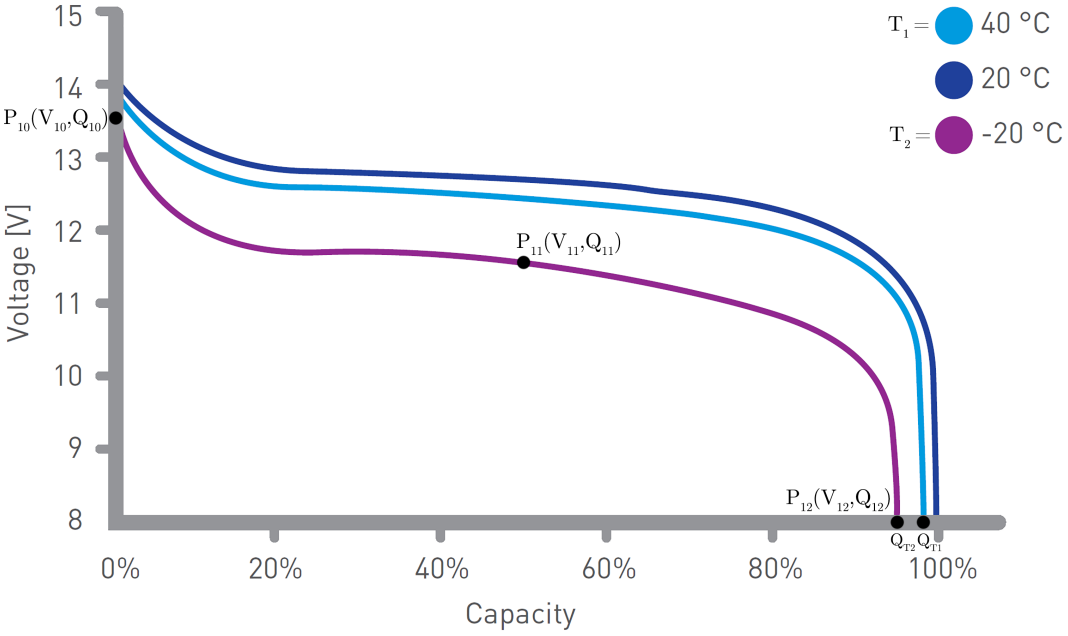

Figure 3.7: Selected points for discharge data at different temperatures used in this thesis.

i_T. The points $P_{10}(V_{10}, Q_{10}) \ldots P_{12}(V_{12}, Q_{12})$ are marked on fig. 3.7. Not to bore the reader, we refer yet again to the original paper for the derivation and here the matrix equation as well, as the procedure is the same as above.

3.5 Modification for batteries in series & parallel

For modelling systems with more than one battery pack, which is necessary in most cases, we modify the model as described in table 3.1. The variables N_{ser} and N_{par} are the number of batteries in series in each string and the number of strings in parallel respectively.

3.6 Implementation in the Simulink environment

For the implementation of the battery model, the Simulink environment was chosen. Simulink is a graphical programming environment for modelling, simulating and analysing multi-domain dynamical systems [43]. It is developed by MathWorks and is an integrated part of the MATLAB software suite, meaning it is possible to run code written in the MATLAB language in SIMULINK. This environment was chosen as it is specifically targeted and optimised for

Table 3.1: Modification of battery parameters for battery systems with more than one battery pack.

Parameter	Modification
Nominal voltage	$V_0 \cdot N_{ser}$
Internal resistance	$R_0 \cdot N_{ser}/N_{par}$
Polarization	$K_0 \cdot N_{ser}$
Exponential zone voltage constant	$A_0 \cdot N_{ser}$
Exponential zone inverse time constant	$B \cdot N_{par}$
Rated capacity	$Q_0 \cdot N_{par}$
Nominal discharge current	$i_0 \cdot N_{par}$

system modelling, is flexible and contains a wide variety of premade electric components. Since this thesis is part of a larger effort in our research group to model more complex energy systems, it was essential to use an environment that easily allows for interaction with other components developed in the same environment in the future. This is not the case with models developed in popular text-based programming languages, such as Python, Java or C(++). It is, however, possible to generate C or C++ code from a SIMULINK model if needed at a later time. Figure 3.8 shows what the underlying structure of the battery model looks like.

The battery model has been made configurable through an interface to make the simple to use for further use and development, as can be seen in fig. 3.9.

3.7 Replication of battery performance

To validate the model accuracy, points from the discharge curves are used to estimate the model parameters. The points (voltage-capacity values) used are reported in table 3.2.

Applying the procedure from section 3.4, we find an estimation for the optimum values of the model parameters. These are reported in table 3.3.

To test the validity of the implemented battery model, we compare the output from our model with the original data from Nilar AB [22] in fig. 3.10 and fig. 3.11. We observe as expected that the model is able to capture the features of interest with high accuracy (less than 0.6% around area of interest), although showing higher deviation (up to 3%), particularly at the end of the nominal zone (8-9V area).

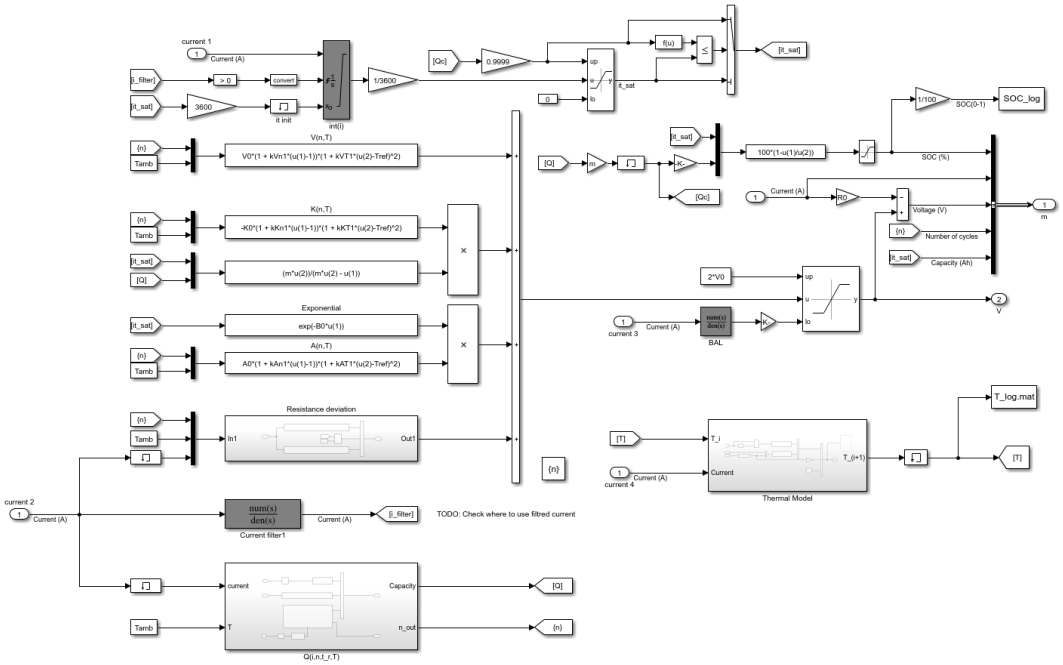

Figure 3.8: Overview of the battery model implementation.

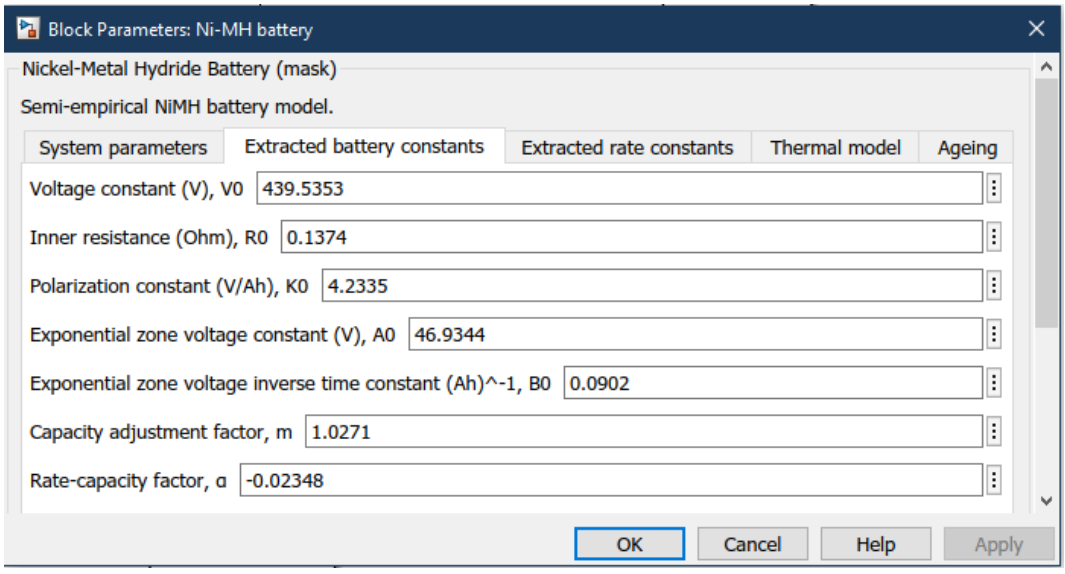

Figure 3.9: User interface for interacting with the battery model.

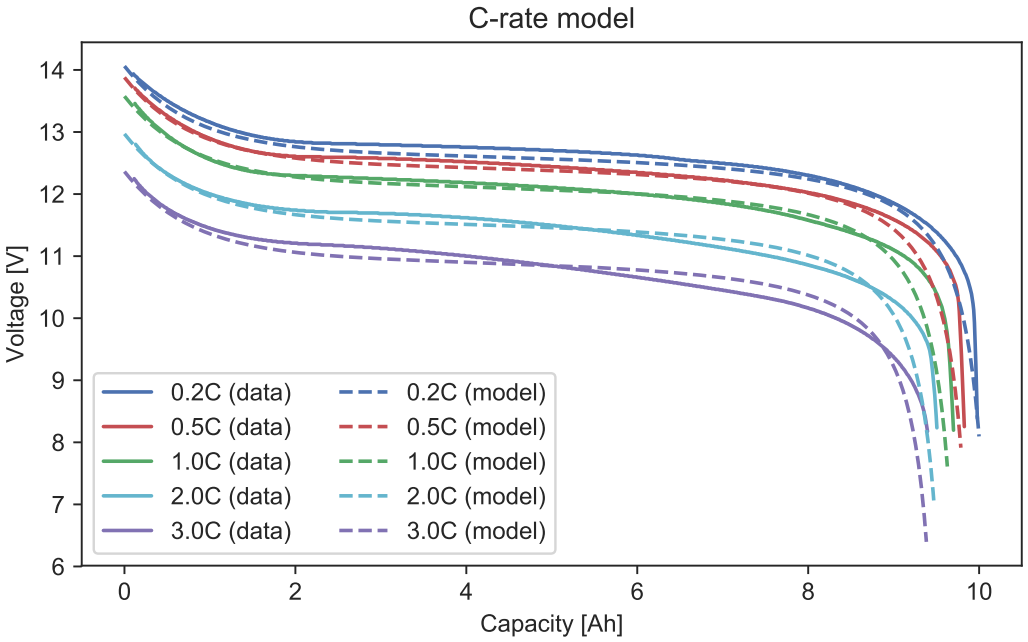

Figure 3.10: Comparison of real discharge data for varying c-rates compared with model output.

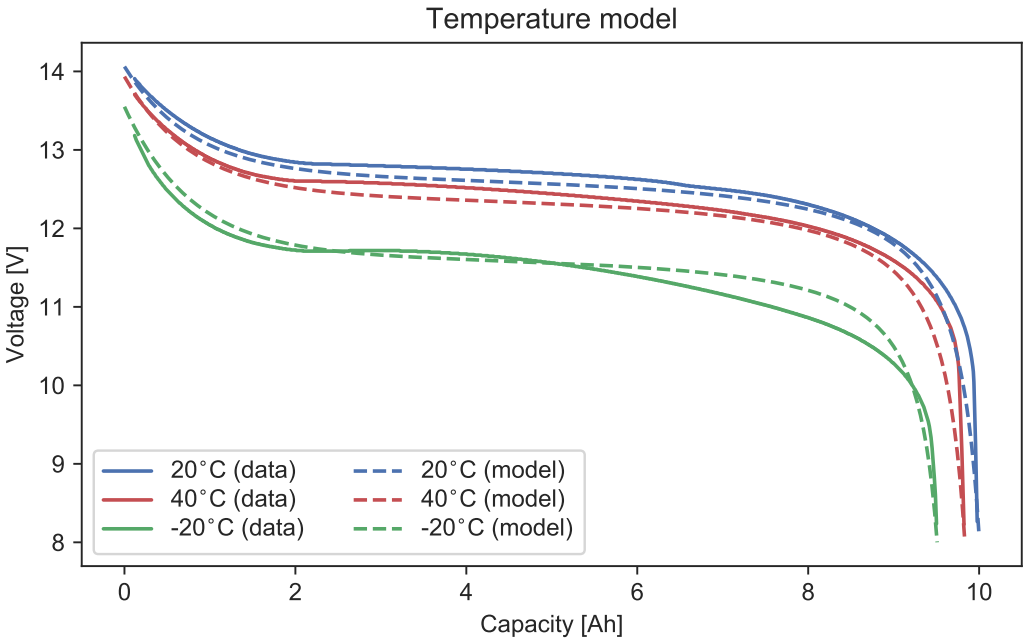

Figure 3.11: Comparison of real discharge data for varying discharge temperatures compared with model output.

Table 3.2: Selected points from voltage curves for a NiMH Nilar EC battery

Point	Voltage (V)	Capacity (A h)
P_1	13.88	0.00
P_2	12.89	1.00
P_3	12.61	2.00
P_4	12.02	8.02
P_5	8.00	9.83
P_6	11.49	5.04
P_7	13.42	0.00
P_8	12.62	4.75
P_9	8.00	8.60
P_{10}	13.55	0.00
P_{11}	11.56	5.00
P_{12}	8.00	9.51

Table 3.3: Estimated parameters from battery discharge curves.

Parameter (Unit)	Value	Parameter	Value (Unit)
V_0 (V)	12.928	k_{VT_1}	$-6.7072 \cdot 10^{-5}$
R_0 (Ω)	0.0607	k_{RT_1}	-0.0018
K_0 (V)	0.1245	k_{KT_1}	$-1.2611 \cdot 10^{-4}$
A_0 (V)	1.3804	k_{AT_1}	$2.3035 \cdot 10^{-4}$
B (A h)$^{-1}$	1.2629	k_{Vn_1}	$5.6429 \cdot 10^{-5}$
m	1.0271	k_{Rn_1}	$6.4908 \cdot 10^{-4}$
α	-0.0235	k_{Kn_1}	$2.8910 \cdot 10^{-5}$
k_{QT_1}	$2.3035 \cdot 10^{-4}$	k_{An_1}	$-3.8318 \cdot 10^{-4}$
k_{QT_2}	$2.3035 \cdot 10^{-4}$		

4 System scenario

In this chapter, we consider the feasibility of powering an EV charging station that is operating in island mode, meaning it is disconnected from the grid, with renewable energy sources. By combining multiple intermittent energy sources with energy backup, we explore the potential of reducing the individual drawbacks of each energy source. The system is connected to a BESS consisting of NiMH batteries which absorb energy from the RES most of the time, and delivers a high burst of power when one or more EVs are charging.

First, the system setup and the details of the BESS is described. Further, we describe the data used in the simulation, although some features have been presented under an NDA. Also, we consider several different scenarios and explore the impact of various parameters in our system, including the impact of usage patterns, energy mix, battery capacity and RES capacity. At last, the results are discussed, and we conclude with some relevant remarks.

4.1 System description

The hybrid renewable energy system considered consists of the following four components:

- Wind turbine
- PV system
- Multi-standard EV-charging station
- NiMH battery energy storage system

In general, when connecting such components, one has to include various power electronics depending on the configuration and the particular requirements of the application. This can include converters, inverters, PID controllers, transient suppressing devices, and so on. When designing systems, one can model the behaviour of each of these to ensure that they work as expected. However, such behaviour is typically simulated at very small timescales, as they require high time resolutions to observe the phenomenons of interest. Since we in this thesis are interested in considering the overall feasibility of the system, not the details of the power electronics, we assume that these components work as expected to get acceptable simulation speeds.

The full system, including battery management system (BMS), was implemented in the Simulink environment.

4.2 Battery energy storage system description

The building block of the battery energy storage system system is the 12 V Nilar EC module which has been referred to throughout the thesis. One module consists of 10 battery cells in series (each of 1.2 V), with a rated capacity of 10 Ah. To achieve a voltage of 408 V, modules are arranged in strings of 34. Further, 14 strings are arranged in parallel to give a total capacity of 140 Ah. The total energy is then equal to 57.6 kW h, which is equivalent to one large battery rack available from Nilar. The battery model constants are modified according to section 3.5. Note here that in reality, one would buy multiple battery packs, consisting of, e.g. 8-12 modules, and arrange these in series and parallel, not all the individual cells after each-other, but for the current-voltage model, this makes no difference.

Considering only the weight of the battery modules themselves, and not the racks or casing, the total mass of the batteries is 1240kg. The overall heat transfer coefficient between the battery surface and its surrounding fluid can be changed depending on the cooling method of the BESS. In this scenario, we assume a heat transfer coefficient of 35 $\mathrm{W/(m^2\,K)}$ on all sides of the rack, except the bottom, which is equivalent to a modest forced convection value with air [41]. Considering the size of the rack, the total surface area is 9.3 $\mathrm{m^2}$ [44].

The overall heat capacity is difficult to estimate based only on information provided by the manufacturer. Assuming the heat capacity will be in a similar range as other NiMH batteries which have previously been measured (ranging from $520-790\,\mathrm{J/(kg\,K)}$ [45]) a value towards the higher end of the range is selected, as larger battery modules have less relative packaging

than their smaller counterparts. This parameter can, of course, be changed if one can obtain more accurate data, or can conduct measurements. A summary of the parameters used for the BESS in this scenario is found in table 4.1. The remaining battery parameters have been scaled according to section 3.5.

Table 4.1: Parameters used for battery system and ageing model.

Parameter (Unit)	Value
Initial SOC (%)	100
Nominal Voltage (V)	408
Rated capacity (A h)	140
Reference discharge current (A)	28
Battery mass (kg)	1238 [44]
Ambient temperature (°C)	30
Inner resistance onset cycle-number	600 [24]
end of life capacity (%)	80 [22]
Optimum temperature (°C)	20 [15]
Cycle-life loss per degree above optimum temperature (%)	2 [15]
Cycle-life parameter β	1.526 [44]
Cycle-life parameter C	0.0005564 [44]
Weighted-average module heat capacity (J/(kg K))	700 [45]
Overall heat transfer coefficient (W/K)	10.60 [41, 44]

4.2.1 Description of wind data

A Norwegian power production company provided wind power production data for one wind-turbine from the year of 2017. The data was sampled with a 10-minute resolution. A subset of the data is shown in fig. 4.1. Note that the power has been normalised to provide data anonymity.

The power output is scaled to produce a particular total energy output throughout the simulation, as described in each scenario.

4.2.2 Description of solar data

PV power production data were obtained from SolarEdge Technologies Inc. – a provider of PV inverters and PV monitoring systems. Data was chosen from a location near the wind

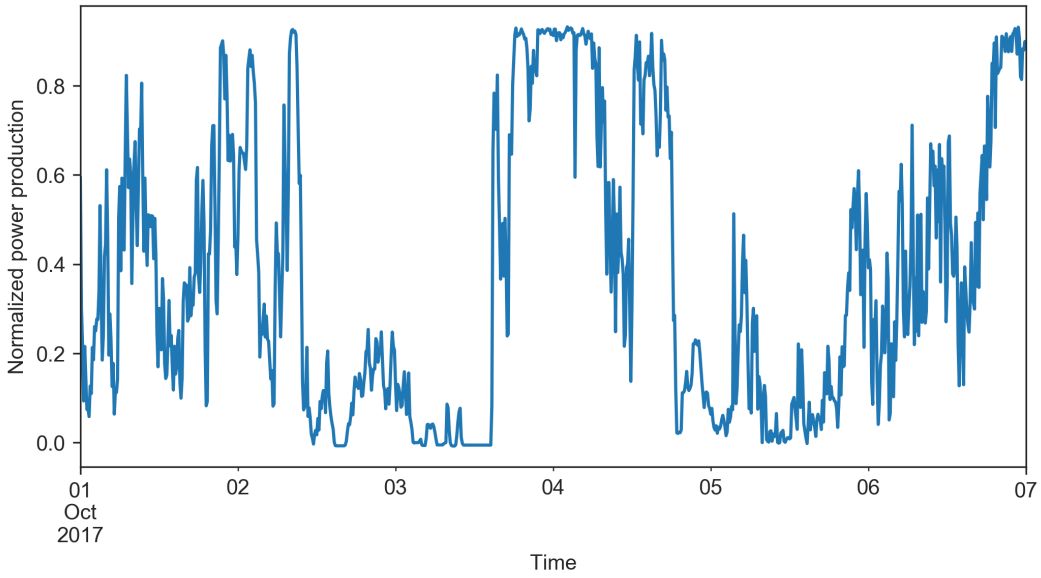

Figure 4.1: Wind power production for one week in October 2017.

power facility to provide a realistic scenario. The data was sampled with a 15-minute resolution for the year 2018. A subset of the data is shown in fig. 4.2. Note that the power is normalised here as well.

4.2.3 Charging station data

EV charging data was obtained for a multi-standard charging station, supporting Combo (CCS), CHAdeMO and AC charging standards. Table 4.2 details the maximum available output at the given station. Note that the charging standards themselves do support higher theoretical output than available for this specific charging station. Further details regarding location and other specifics are disclosed.

Table 4.2: Charging standards available at the given charging station in the data set [46]

Standard	Max Voltage	Max Power
Combined Charging System (CCS) (DC)	400V	<50kW (125A)
CHAdeMO (DC)	400V	<50kW (125A)
AC (3 phase)	400V	<22kW (32A)

Since the EV charging data did not contain the actual power output over time, it had to be transformed into a time-series format based on some assumptions described in the follow-

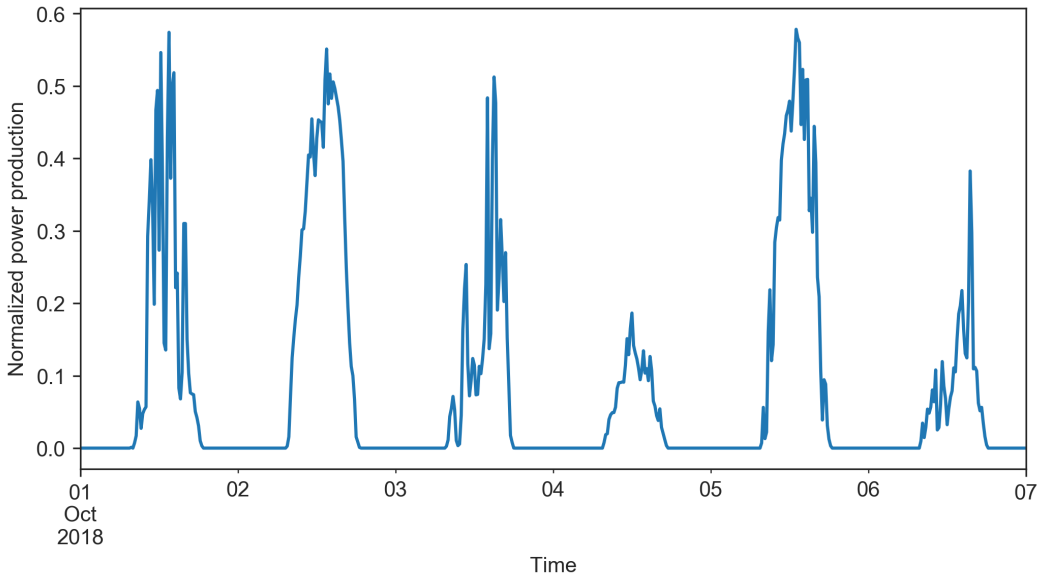

Figure 4.2: Solar power production in one week in October 2018.

ing. A sample of the data is shown in table 4.3. The data do not indicate at which time during an hour a car is charged. However, if *#CHARGING = 0*, this suggests that a vehicle has continued to charge since the previous hour. We have then assigned these cars to the beginning of the hour. The script for transforming the data set to time-series is provided in appendix A.

Table 4.3: Sample of EV charging data.

DATETIME	TIME(S)	#CHARGING	TYPE
⋮	⋮	⋮	⋮
01/09/2017 11:00	1392	0	CHAdeMO
01/09/2017 11:00	867	1	CCS
01/09/2017 12:00	279	1	CHAdeMO
01/09/2017 13:00	1039	0	CHAdeMO
01/09/2017 15:00	2009	1	CHAdeMO
01/09/2017 15:00	453	1	AC
⋮	⋮	⋮	⋮

In real life, an EV charger is never going to deliver the maximum theoretical output throughout the entire charging session. It might come close only if charging under optimal conditions– at the right temperature and during the first part of the recharge, given the state of charge (SOC) is low. During winter in Norway, one is likely to get a much lower output than rated,

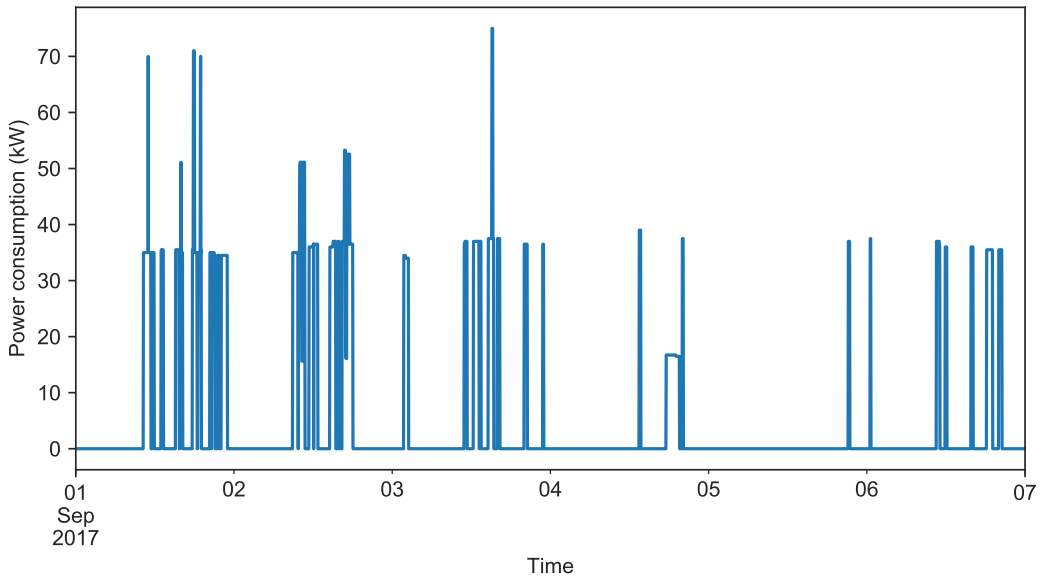

Figure 4.3: Sample of electrical vehicle time series for one week in September 2017

so charging times will typically be longer than during summer. We, therefore, estimate the influence of temperature on the power output. Trentadue *et al.* measured the effect of temperature on the delivered power from multi-type fast-charging stations, showing a clear linear decrease from 90% of the theoretical output to around 10% at −25 °C [47]. Using hourly temperature data available through Frost API by the Norwegian Meteorological Institute, we thereby modify the output accordingly.

As mentioned, the rate of charge is typically fast at the beginning of the charging process and decreases towards the end of the charge [48]. The characteristics of this effect vary significantly from car to car, and because we do not have information about the type of car charging, nor their original SOC when arriving at the charging station, we have not been able to include this effect when converting the data to time-series format.

In the obtained data set, there is a clear trend regarding seasonality, as shown in fig. 4.4. This is a likely distribution for some EV-charging stations, but other charging stations might be placed geographically in such a way that there are not any observable seasonal trends.

For this reason, a hypothetical data set was created for a second charging station. This was done by randomising days from average months in the original data set and ensuring the same total energy consumption over the year. As can be seen in fig. 4.5, there is still some variation between the months, but no seasonality trend.

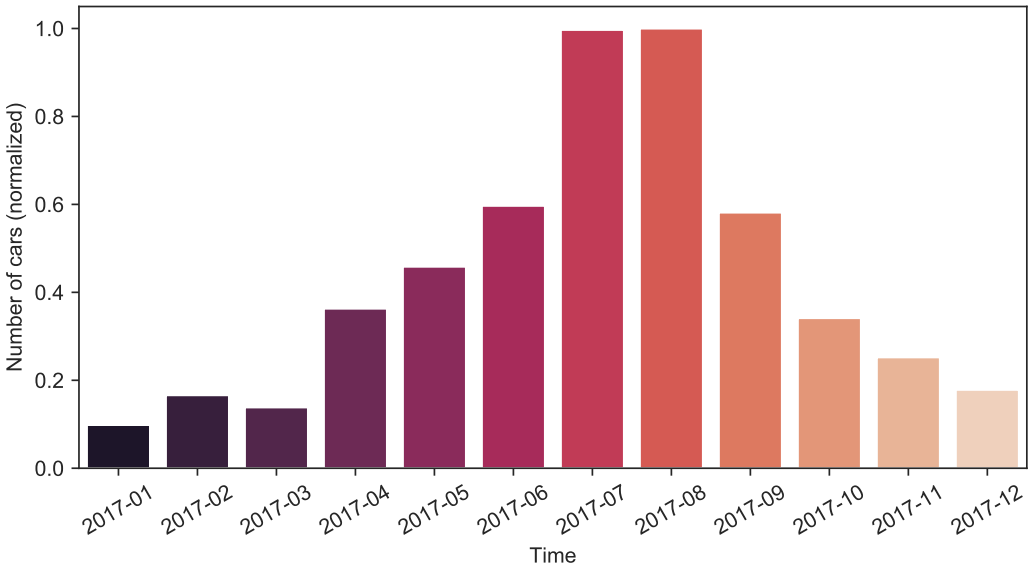

Figure 4.4: Number of cars per month in the original data set, normalised for anonymity.

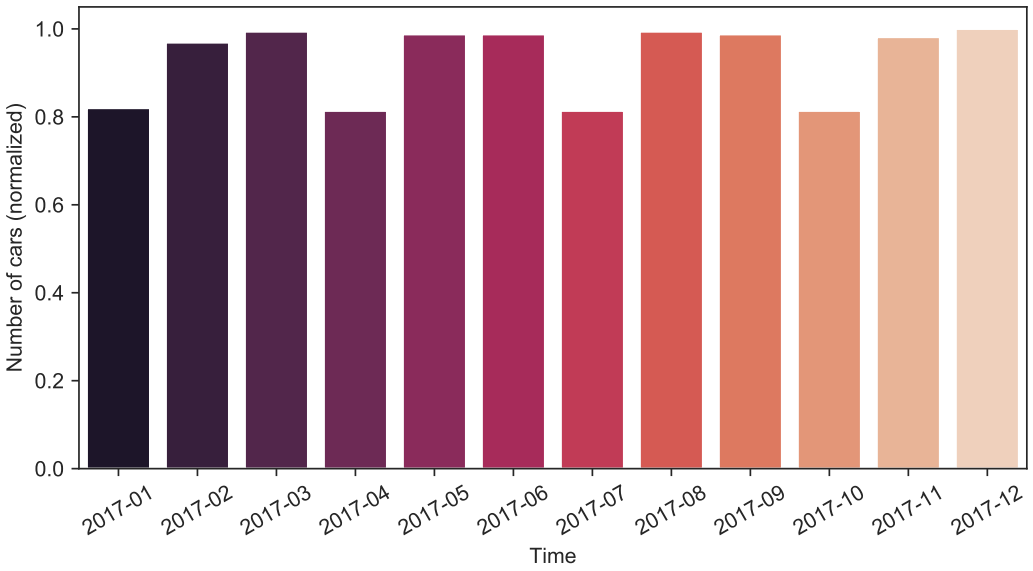

Figure 4.5: Number of cars per month in the original data set, normalised for anonymity.

4.3 Control System

A battery energy storage system (BESS) is always controlled by a BMS to ensure safe operation. Protecting the battery from operating outside its safe operating area is done by continuously monitoring voltage, current, capacity etc. A control system for the battery system was implemented according to the manufacturer's recommendations, to ensure safe charging behaviour. The recommended SOC range is $5\% \leq SOC \leq 95\%$, which is approximately equal to a cut-off voltage of 80% of the midpoint voltage. The maximum discharge rate is set to $5C = 700A$, and the maximum charging rate to $0.5C = 70A$. For this set-up, the maximum discharge rate is never exceeded as it is well above the maximum drain from the EV charging station.

Since we impose power curtailment in an island-mode energy system, energy goes to waste when the amount of power produced by the RESs cannot be absorbed by the battery, nor the EV charging station. In the opposite case, when the battery SOC is below the minimum threshold, and the amount demand by the charging station exceeds what is produced by the RESs, the excess load has to be cut off.

4.4 Scenario results & discussion

The total amount of energy which is not utilised (power curtailment), and the total amount of energy not provided (load shed) is monitored by the control system throughout the simulation and reported along with the estimated cycle-age after one year. The total amount of power produced is set to be the same in all considered scenarios if nothing else is stated to make the results comparable. The total amount of electricity produced is chosen to be equal to the total amount of energy consumed throughout the simulation.

The system is simulated for one year with a time resolution of 1 minute. Performance decrease due to ageing is updated once every 24 hours to increase simulation speed.

4.4.1 Scenario 1 – Only wind

First, we consider a scenario where the two charging stations are powered only by energy produced from wind. The simulation results for both stations are reported in section 4.4.2.

Data set	Energy from wind	Energy from solar	Cycle-age	Curtailment	Load shed
Original	100%	0%	109	58%	57%
Hypothetical	100%	0%	153	47%	43%

Since power production from wind on average is the same during the year, we see that this configuration favours the hypothetical charging station. However, as half of the energy is wasted, and half of the consumption cannot be provided, this scenario cannot be considered a good match for either of the charging stations. The increase in cycle-age for the station where more energy is utilised is in line with what is expected.

4.4.2 Scenario 2 – Only solar

Similarly, a scenario where all energy is produced by solar power is considered. Section 4.4.2 summarises the simulation outputs from both charging stations.

Data set	Energy from wind	Energy from solar	Cycle-age	Curtailment	Load shed
Original	0%	100%	145	35%	34%
Hypothetical	0%	100%	145	43%	40%

For this scenario, it is clear that the original charging station, at which most power is consumed during the summer months, is favoured. The production/consumption pattern is however not a perfect fit, as the number of cars charging is at its highest in August, and the power production from solar peaks in June when days are the longest. The synthetic charging station can deliver more power and waste less in this scenario as well. Still, the amount of undelivered and wasted energy is too high to be considered a good fit.

4.4.3 Scenario 3 – Combination of solar & wind

In theory, it should be possible to alleviate the individual drawbacks of one renewable energy source, by combining it with other sources which exhibit different production patterns over the course of the day. By combining different ratios of power from solar and wind, we examine if it is indeed possible to improve performance by considering a mix of energy sources. The findings from these simulations are reported in tables 4.4 and 4.5.

Table 4.4: Simulation results for original charging station.

Energy from wind	Energy from solar	Cycle-age	Curtailment	Load shed
⋮	⋮	⋮	⋮	⋮
40%	60%	145	37%	36%
30%	70%	150	35%	34%
20%	80%	152	34%	32%
10%	90%	149	34%	32%
⋮	⋮	⋮	⋮	⋮

Compared to the pure PV based scenario, it proved possible to improve performance for the original charging station by including roughly 20% of wind energy into the system. This confirms that energy production from wind can at some times be able to increase the amount of delivered energy since power can be produced at night or when it is cloudy.

As the improvement compared to the pure PV powered system is rather small, it might not be preferable to include a small wind turbine from a purely economic standpoint, given that more power electronics would be needed to connect it to the system.

Table 4.5: Simulation results for hypothetical charging station.

Energy from wind	Energy from solar	Cycle-age	Curtailment	Load shed
⋮	⋮	⋮	⋮	⋮
60%	40%	185	34%	31%
50%	50%	186	34%	30%
40%	60%	182	34%	30%
30%	70%	178	34%	31%
⋮	⋮	⋮	⋮	⋮

A more significant improvement is observed by combining energy the two RES for the hypothetical EV-charging station. The ideal combination was found to be approximately a 50/50 mix of the two RES. It is possible that by including the influence of temperature on charging efficiency when converting the data set to a time series, the use of solar power was partially favoured as charging times were not proportionally reduced. Considering this it is possible that the system could benefit from an even higher percentage of the energy coming from wind.

Having found an optimum combination of solar and wind for the two EV-charging stations, we observe that roughly one-third of the energy produced is wasted and one-third of the

load cannot be delivered. Considering that the amount of load shed and power curtailment is quite similar, it is of interest to see how much the size of the BESS and the energy output of the RES would influence the performance.

4.4.4 Influence of battery size

The simulation results in the previous sections considered a BESS with a total energy storage capacity of 57.6 kW h. Fixing the mix of solar and wind to the optimum combination found in section 4.4.3, the effect of increasing battery capacity on curtailment and load shedding is simulated. The results from a BESS with 1.5× and 2.0× are compared to the original capacity in tables 4.6 and 4.7.

Table 4.6: Effect of increasing battery capacity on original charging station performance.

Capacity	Energy from wind	Energy from solar	Cycle-age	Curtailment	Load shed
57.5 kWh	20%	80%	152	35%	33%
86 kWh	20%	80%	96	32%	30%
115 kWh	20%	80%	69	30%	28%

Increasing the capacity of the storage system shows little effect on the original charging station. An absolute decrease of 5% in load shed when doubling the capacity cannot be defended. The reduction in curtailment is found to be equal to the reduction of load-shed, which is correct as it is this extra stored energy that can be utilised with a larger BESS.

Table 4.7: Effect of increasing battery capacity for hypothetical charging station performance.

Capacity	Energy from wind	Energy from solar	Cycle-age	Curtailment	Load shed
57.5 kWh	50%	50%	185	34%	30%
86 kWh	50%	50%	126	28%	24%
115 kWh	50%	50%	95	24%	20%

The effect of increasing capacity is found to be more significant for the hypothetical EV-charging station. A 30% relative improvement in performance is considerable, but also means double the cost spent on batteries. It is not possible to conclude if such an upgrade would be beneficial or not in general for all projects.

4.4.5 Influence of renewable energy production

In previous sections, the total energy production was set to be equal to the total energy consumption over the year. Here we consider scenarios where more energy is produced than what is demanded. Naturally, as the excessive energy has nowhere to go, this will inevitably lead to an increase in power curtailment, but be beneficial for reducing load shed. An increase of 1.2 and 1.5 times the demand is considered, and the simulation results are summarised in tables 4.8 and 4.9.

Table 4.8: Effect of increasing energy production for the original charging station.

Energy production	Energy from wind	Energy from solar	Cycle-age	Curtailment	Load shed
1.0 × consumption	20%	80%	152%	35%	33%
1.2 × consumption	20%	80%	159%	40%	27%
1.5 × consumption	20%	80%	163%	49%	21%

Producing precisely the same amount of energy as what is consumed means that to deliver 100% of the load, no energy could be wasted. For this to happen, one would have to consider a BESS capacity larger than the maximum peak in consumption for the year, which is entirely unrealistic. Also, due to self-discharge and losses, one should always consider *some* over-sizing. It is therefore not surprising to see that an increase in power production also has a substantial, positive effect on performance. Considering the decrease in price per kW in later years, one should seriously consider if this is possible to afford, especially if it is realistic that the system can be connected to the grid at a later point as it would be possible to sell the excess energy.

Table 4.9: Effect of increasing battery capacity for hypothetical charging station.

Energy production	Energy from wind	Energy from solar	Cycle-age	Curtailment	Load shed
1.0 × consumption	50%	50%	185%	34%	30%
1.2 × consumption	50%	50%	190%	41%	26%
1.5 × consumption	50%	50%	191%	50%	22%

The relative improvement is smaller for the hypothetical charging station, but the effect of over-sizing the production by 1.5 times is still much larger than the effect of increasing the storage system by 1.5 times.

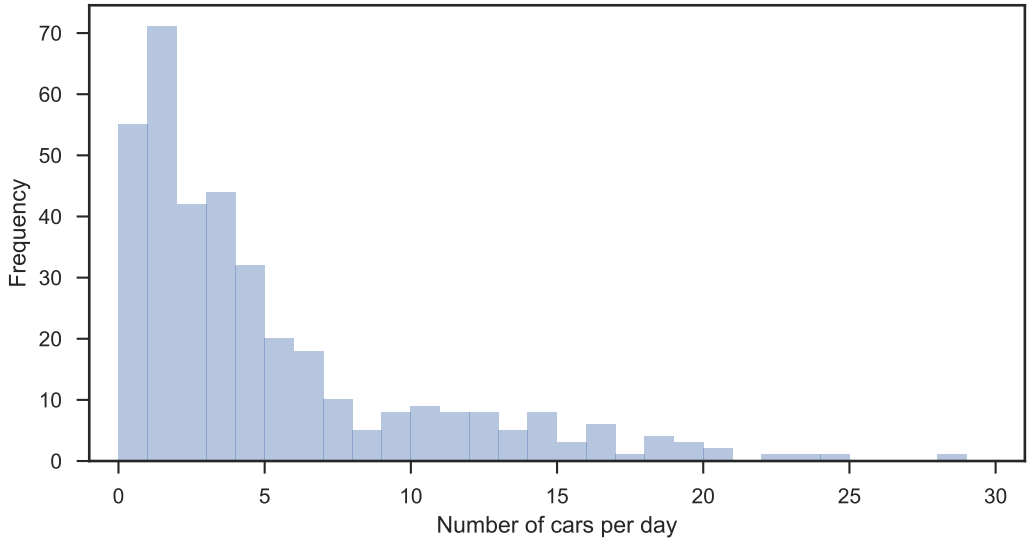

Figure 4.6: Frequency distribution of the number of cars arriving at the charging station per day.

4.4.6 Simulation discussion

It is necessary to take a closer look at the underlying data set, to get a better understanding of the simulation results. In fig. 4.6, the distribution of the number of cars arriving at the charging station per day is shown. We see that most days the number of vehicles coming are in between 1-5. However, it also happens frequently that more than ten cars arrive per day, up to a maximum of 28. To scale power production and storage to provide for the most intensive days would not be economically viable, but then a lot of power also cannot be delivered as the battery runs empty early during the day and never has the time to fill up. It could likely be economically favourable to connect it to the grid, even in a more remote area, considering the periodically heavy use of this charging station.

Figure 4.7 contains a snapshot of the sum of power production and power demand (or current, to be precise) for two days in July, which showcases this problem in more detail. Here we see how cars arrive continuously at the charging station throughout the whole of the 23rd of July, which happens to be a Sunday, while only three cars come on Sunday.

It would've been trivial to fabricate a data set with a more narrow distribution of the number of cars charging per day, as well as to distribute these cars evenly over the day. While we assume that charging stations with more favourable charging patterns than for our charging

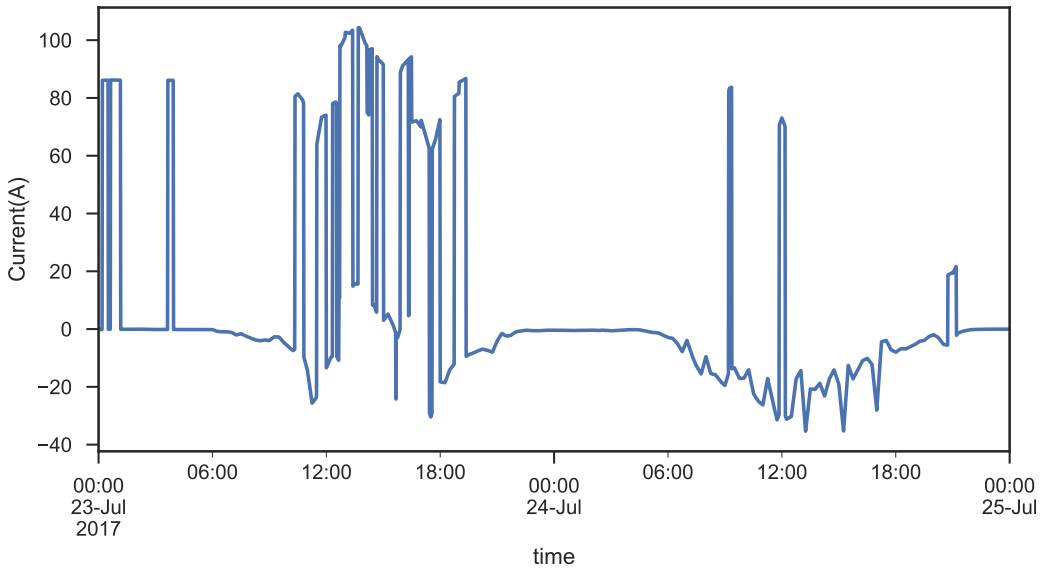

Figure 4.7: Sum of current from PV panels and charging station. Negative numbers indicate that more current is delivered than what is demanded. The plot is from the simulation of the original charging station powered by 100% solar energy.

stations exist, we chose not to create such a data set. Fabricating a time series would be of little value without data to back it up.

As mentioned, the EV charging data set did not contain enough information to reproduce an accurate time series, and we had to make several assumptions in our conversion. This can be considered one of the primary sources of error in this simulation. Since the charging power had to be regarded as the same during the entire period of discharge, and since real EVs reduce the charging power towards the end of the charging period, it is likely that the same charging station connected to the configuration in mention would perform better than what is implied by the simulation results. Based on our experience acquiring data, it might seem like storing this type of data is not common practice for most service providers.

While the EV charging data sets might have been unfavourable for the use case, power production data for the wind turbine might be partly biased in a positive direction. As data was acquired from a large power production company, the site of the wind turbine is likely to be somewhat more ideal than what is available close to the average EV charging site. The data set for the PV system came from a smaller, local provider, and is less likely to contain any bias.

Considering the cycle-life after one year, the simulation results for most of the scenarios considered indicate a BESS of roughly ten years, given that it can deliver the promised cycle life of 1800-2000 cycles. It is necessary to conduct actual measurements over a long period to validate this. While time-consuming, ageing measurements are of considerable interest, as they are still the best sources for creating ageing models. Given the disproportionate amount of such data found in the literature for NiMH batteries compared to what has been published on Li-ion, this would be an essential contribution.

4.5 Future outlook

Since it is not possible to plan and optimise charging times by scheduling them at times with more energy available, one could consider the trying to modifying user behaviour indirectly. In the future, it is for example possible to envision a solution similar to the city-bike system for EV-charging stations, where users could see in real-time the current availability of charging options, as well as the amount of available power for a charging station powered by RES. It would then be possible for users to update and change their charging plan as they travel. This behaviour could further be incentivized through variable charging price, depending on the amount of energy available, making it cheaper for users to charge at charging stations with more power available. In the case where there are plenty of charging stations available, it would be simple for users to pick the one with the highest capacity. In the situation where the charging station is the only one for miles and miles, such indirect user behaviour modification would most likely have a smaller effect.

With the current rapid increase in usage and the electrification of not only passenger cars but also larger vehicles meant for transportation of goods, it is easy to see how usage patterns for EV-charging stations might change considerably in the future. As became evident from our simulation results, a change in charging power could change the optimum power mix between different renewable energy sources and decrease the performance of the system considerably. It will, therefore, be necessary for EV-charging providers to be able to predict changes in charging patterns when considering the design of future charging stations powered by RES

This rapid increase in usage means it might not take long before the capacity of the charging station becomes too small, although satisfactory initially. This problem will continue to incentivizes the use of BESSs in the future. Due to the modular nature of batteries, it makes it

simple to increase the capacity of the system as the demand increases. The same thing could be done by adding PV panels or new wind turbines.

Considering the findings from our simulation, we would like to propose another potential use case for BESS in the future. As of today, nonresidential customers must pay a power tariff when connected to the power grid. This tariff is typically based on the hour in the month with the highest power consumption. Since the point of fast charging stations is to provide high power, this can make it non-viable economically to establish a charging station in a rural area [49] where very few cars pass by, but the maximum consumption is still high for short periods. To lower the cost of power tariff, one can imagine connecting the BESS to the grid using a large inverter, and charge the battery during times of low consumption. Then, one could combine energy from the grid and the BESS when e.g. more than one car is charging, in order not to increase the maximum consumption above a certain threshold, thereby lowering the power tariff. It would be possible to optimise the viability of such a configuration further by letting the battery charge at times when electricity prices are lower.

Lastly, we would like to mention a very recent but promising breakthrough that could be a game-changer for in NiMH-based BESS. In April 2019, Nilar officially announced an improvement in NiMH battery technology that promises "unparalleled energy storage life" [50]. The original research was published in 2018 by Shen *et al.*, who showed that by adding oxygen to the common gas space in the battery pack, it was possible to regain lost electrolyte [24], and thereby restore battery capacity and lower internal resistance to values close to a new system. It remains to see how many times this process can be repeated, but with an already extensive cycle-life, it makes NiMH batteries an even better candidate for BESSs in the future, as the price *per cycle* would be decreased dramatically.

5 Conclusions & Further Work

This chapter summarises the content of this thesis, including the main findings along with their impact. Finally, we end with some thoughts regarding interesting directions for further work on the topic.

5.1 Conclusions

In this thesis, we looked at how the significant increase in energy demand from the electrification of the transportation sector can be met by using renewable energy only. In particular, we have simulated how off-grid EV-charging stations can be powered using energy produced by solar and wind power, and how this configuration benefits from energy storage to help alleviate the intermittent and variable nature of the renewable energy sources.

To be able to simulate this with reasonable accuracy, we developed a flexible, semi-empirical battery energy storage model, that is both capable of capturing performance-degrading effects, such as the influence of temperature on the dynamic response, capacity and current-voltage behaviour, the rate-capacity effect, the influence of useage on ageing, and the influence of battery ageing on system performance. We were still able to obtain reasonable simulation speeds (10 minutes for our system simulation). This is a substantial difference compared to battery models typically used for system simulations in the literature, which do not consider these types of effects. The proposed model was calibrated by using data from nickel-metal hydride based battery storage system, to consider this chemistry as a candidate to the currently more popular Li-ion-based battery energy storage systems. As input to the system simulation, real data from Norwegian renewable energy producers and a Norwegian EV charging operator was used.

Our simulations showed how the performance of the system in mention could benefit from combining more than one renewable energy source. The effectiveness of this approach was

shown to depend on the usage pattern of the particular EV-charging station, with best performances (ten% improvement) obtained for the charging station which did not show a trend in seasonality, as the original charging station already fit well with the production pattern from PV. A performance dependency on the sporadicity of cars charging cars was observed from the data, and we conclude that more irregular charging patterns benefit the storage system, as it is able to restore more energy during idle periods, thereby meeting a larger percentage of the demand.

Further, the simulation results showed that improvements in performance from increasing storage capacity by 1.5 times, was in the range of 3-6%. On the other side, the impact of up-scaling power production by RES by 1.5 times, had up to 8-12% improvement on reducing load shed. With this type of information when considering system upgrades, decision-makers are better suited to pick the most beneficial choice.

Finally, we found the NiMH-based storage system to be a viable alternative to Li-ion-based systems, as simulation results indicated a ten-year lifetime for the NiMH battery energy storage system. Furthermore, recent research suggests it might be possible to prolong the lifetime of NiMH batteries far beyond what has been previously possible. This only strengthens the argument for considering this chemistry as part of the solution to solving the climate crisis.

5.2 Further work

The best way to test the BESS model and the system model would be in a real test facility. Currently, one has to go abroad to get access to such facilities. The energy storage system research group where this thesis has been performed has acquired funding to build a small-scale facility in the next years. It will, therefore, be possible to try and validate the models. Here one could also acquire battery test data with much higher resolution than what has been considered in this thesis.

As a further development of the system model, it could be extended to include a limited grid-connection to test the use case outlined in the latter part of section 4.4.6, and conduct an optimisation of the charging algorithm based on electricity price and price predictions to reduce costs.

It would also be of interest to attack the problems outlined this thesis from a different direction. For instance, instead of trying to optimise the system configuration based on the

location, one could estimate the most suitable sites for a given configuration. This could be done by combining Norwegian traffic data, made openly accessible by The Norwegian Public Roads Administration at , with meteorological data made publicly available by the Norwegian Meteorological Institute at .

Finally, taking into consideration how difficult it has proven to obtain data from service providers, it would be a good idea to consider collaborations with a set of industrial partners in the near future. The availability of large data sets of good quality is without a doubt of out-most importance for research on the topic in the coming years.

A Code

A.1 EV-script

```
# Imports
import pandas as pd
import numpy as np

# Load data
EV_data = pd.read_excel('Ladestasjon_2017.xlsx')
EV_data.columns = ['Time','time(s)','#charging','type']
EV_data['Time'] = pd.to_datetime(EV_data['Time'], dayfirst=True)

T_data = pd.read_csv('temperature.csv')
T_data.columns = ['Temperature(C)','Time']
T_data['Time'] = pd.to_datetime(T_data['Time'])
T_data = T_data.set_index('Time')

# Extract hours when #charging = 0
EV_data = EV_data.replace(0, np.nan)
null_data = EV_data[EV_data['#charging'].isnull()]
null_data = null_data.replace(np.nan, 0)

# Separate data when #charging != 0
other_data = EV_data.dropna()

# Group instances when there are multiple charging events
# of same type in one hour
other_data = other_data.groupby(['Time', 'type'], as_index=False).sum()

# Combine null_data and other_data and set Time as index
EV_data = pd.merge_ordered(other_data, null_data)
EV_data['#charging'] = EV_data['#charging'].astype('int32')
```

```
EV_data = EV_data[['Time','time(s)','#charging','type']]
EV_data = EV_data.set_index('Time')

# Function to check if charging continues next hour
def hasNext(df, currentindex, currentrow):
    hasNext = False
    currenttype = currentrow['type']
    nexttime = currentindex + pd.Timedelta(hours=1)

    if nexttime in EV_data.index:
        item = EV_data.loc[nexttime]
        if isinstance(item, pd.core.frame.DataFrame):
            for index, row in item.iterrows():
                if row['type'] == currenttype:
                    hasNext = True
        else:
            if item['type'] == currenttype:
                hasNext = True

    return hasNext

# Function to add temperature effect
def temperatureEffect(temp):
    if temp >= 25:
        return 0.9
    elif temp < -25:
        return 0.1
    else:
        return round(temp*0.016 + 0.5, 2)

# Convert to timeseries
idx = pd.date_range('2017-01-01', '2018-01-01', freq='min')
ts = pd.DataFrame([0]*len(idx),columns=['Current(A)'])
ts['Time'] = idx
ts = ts.set_index('Time')

for index, row in EV_data.iterrows():
    min = round(row['time(s)']/60)

    if row['type'] == 'AC':
        I = 32 * temperatureEffect(T_data.loc[index]['Temperature(C)'])
```

```
    elif row['type'] == 'CHAdeMO':
        I = 125 * temperatureEffect(T_data.loc[index]['Temperature(C)'])
    elif row['type'] == 'CCS':
        I = 125 * temperatureEffect(T_data.loc[index]['Temperature(C)'])

    # Select intra-hour starting time based on other information
    # Case 1: Started charging previous hour
    if row['#charging'] == 0:
        loc = ts.index.get_loc(index)
        ts.iloc[range(loc,loc+min)] += I
    # Case 2: Will continue to charge next hour
    elif hasNext(EV_data, index, row):
        loc = ts.index.get_loc(index) + (60 - min)
        ts.iloc[range(loc,loc+min)] += I
    # Case 3: Will not continue to charge next hour
    else:
        if min == 60:
            loc = ts.index.get_loc(index)
            ts.iloc[range(loc,loc+min)] += I
        else:
            loc = ts.index.get_loc(index) + np.random.randint(60 - min)
            ts.iloc[range(loc,loc+min)] += I

ts.to_csv('original_timeseries.csv')
```

Listing 1: Python-script for converting ev-data to timeseries.

A.2 Script for calculating NiMH-battery model parameters

```
%% Set number of batteries (not cells)
N_ser = 1; % Number of batteries in series (multiple of 12V)
N_par = 1; % Number of battery strings in parallel (multiple of 10Ah)

%% Extracted points and values from discharge curve data
%% Define list of points here ...

%% Compute initial constants
alpha = log10(Qi2/Qi1)/log10(i2/i1);
B0 = -(1/Q2)*log(((Vfull - V3)/(Vfull - V2)) - 1);
A0 = (Vfull - V3)/(1 - exp(-B0*Q3));
```

```
s1 = Vfull - V4 - A0*(1 - exp(-B0*Q4));
s2 = Vfull - V5 - A0*(1 - exp(-B0*Q5));
m  = ((1 - (s2)/(s1))/(1 - (s2*Q4)/(s1*Q5))) * (Q4/Qi1);
K0 = s2*(m*(Qi1/Q5) - 1);
R0 = (1/(i1 - i2))*(V6 + K0*(m*Qi2/(m*Qi2 - Q6)) - A0*exp(-B0*Q6) ...
       - (V3 + K0*((m*Qi1)/(m*Qi1 - Q3)) - A0*exp(-B0*Q3)));
V0 = Vfull + R0*i1 + K0 - A0;

%% Compute first-order rate constants affecting capacity degradation
AQn = 0.5*[(n1-1)*n1  (n1-1)*n1*(2*n1-1)
           (n2-1)*n2  (n2-1)*n2*(2*n2-1)];

bQn = [Qn1/(Q0*(in/i0)^alpha) - 1
       Qn2/(Q0*(in/i0)^alpha) - 1];

kQn = AQn\bQn;
kQn1 = kQn(1);
kQn2 = kQn(2);

AQT = [T1 - Tref  (T1 - Tref)^2
       T2 - Tref  (T2 - Tref)^2];

bQT = [QT1/(Q0*(iT/i0)^alpha) - 1
       QT2/(Q0*(iT/i0)^alpha) - 1];

kQT = AQT\bQT;
kQT1 = kQT(1);
kQT2 = kQT(2);

%% Compute first-order rate constants affecting initial constants
Q = Q0*(in/i0)^alpha * (1 + (n2-1)*n2/2*kQn1 + (n2-1)*n2*(2*n2-1)/2*kQn2);

AXn = [V0        -R0*i1        -K0                      A0
       V0*(n2-1) -R0*in*(n2-1) -K0*(n2-1)               A0*(n2-1)
       V0*(n2-1) -R0*in*(n2-1) -K0*(n2-1)*m*Q/(m*Q-Q8)  A0*(n2-1)*exp(-B0*Q8)
       V0*(n2-1) -R0*in*(n2-1) -K0*(n2-1)*m*Q/(m*Q-Q9)  A0*(n2-1)*exp(-B0*Q9)];

bXn = [Vfull - (V0 - R0*i1 - K0 + A0)
       V7 - (V0 - R0*in - K0 + A0)
       V8 - (V0 - R0*in - K0*m*Q/(m*Q-Q8) + A0*exp(-B0*Q8))
       V9 - (V0 - R0*in - K0*m*Q/(m*Q-Q9) + A0*exp(-B0*Q9))];
```

```
kXn = AXn\bXn;
kVn1 = kXn(1);
kRn1 = kXn(2);
kKn1 = kXn(3);
kAn1 = kXn(4);

Q = Q0*(iT/i0)^alpha * (1 + kQT1*(T2-Tref) + kQT2*(T2 - Tref)^2);

AXT = [V0              -R0*i1              -K0                              A0
       V0*(T2-Tref)^2 -R0*iT*(T2-Tref)^2 -K0*(T2-Tref)^2                  A0*(T2-Tref)^2
       V0*(T2-Tref)^2 -R0*iT*(T2-Tref)^2 -K0*(T2-Tref)^2 * m*Q/(m*Q-Q11) A0*(T2-Tref)^2 * exp(-B0*Q11)
       V0*(T2-Tref)^2 -R0*iT*(T2-Tref)^2 -K0*(T2-Tref)^2 * m*Q/(m*Q-Q12) A0*(T2-Tref)^2 * exp(-B0*Q12)]

bXT = [Vfull - (V0 - R0*i1 - K0 + A0)
       V10   - (V0 - R0*iT - K0 + A0)
       V11   - (V0 - R0*iT - K0*m*Q/(m*Q-Q11) + A0*exp(-B0*Q11))
       V12   - (V0 - R0*iT - K0*m*Q/(m*Q-Q12) + A0*exp(-B0*Q12))];

kXT = AXT\bXT;
kVT2 = kXT(1);
kRT2 = kXT(2);
kKT2 = kXT(3);
kAT2 = kXT(4);

%% Include effect of batteries in series and parallel
A0 = A0*N_ser;
K0 = K0*N_ser;
V0 = V0*N_ser;
R0 = R0*(N_ser/N_par);
B0 = B0/N_par;
i0 = i0*N_par;
Q0 = Q0*N_par;
```

Listing 2: MATLAB-script calculating NiMH-battery model parameters from battery discharge curves.

Glossary

C-rate A measure of the discharge current relative to the battery capacity. Discharging at a C-rate of 1C is equal to discharging the full battery in one hour. For a battery with 10Ah capacity that would mean a discharge current of 10A. For this battery, discharging at 20A would be equal to a discharge rate of 2C. It is useful measure when comparing batteries since batteries are available in a large range of capacities.

Capacity The battery capacity depends on the C-rate and is defined as the product of the time it takes to discharge the battery fully (in hours) multiplied by the discharge current (A). The nominal capacity is defined as the capacity measured for a fresh battery at the nominal discharge current. It should not be confused with the nominal energy, which is the product of the discharge voltage and the nominal battery capacity.

Closed-circuit voltage The cloced-circuit voltage (CCV) is the potential difference measured between the terminals when a load is applied. It often referred to as the terminal voltage. The closed circuit voltage varies depending on the C-rate and SOC.

Cut-off voltage The voltage which defines 0% SOC. The battery is not allowed to be discharged further after reaching this voltage.

Cycle-life The number of full charge-discharge cycles a battery is expected to deliver (cycling at a specific DOD, C-rate and temperature) before it reaches its end of life (EOL).

Depth-of-discharge It is most common to define the depth-of-discharge (DOD) as the inverse of the state-of-charge, meaning a 25% SOC is equal to a 75% DOD. However, there are several different (and sometimes conflicting definitions) found in the literature. The most common of which is to use DOD as a description of the percentage-wise change in SOC from its previous state. According to this definition, discharging a battery from 75% to 25% SOC equals a 50% DOD. In this thesis we refer to the latter as *relative* DOD.

E-rate: Similar to C-rate, but a measure of discharge power. An E-rate of 2E is the power needed to charge or discharge the battery in 30 minutes.

End of life As battery performance sinks below a given performance measure, battery manufacturers recommend that it should be replaced. This is typically when the battery capacity falls below 80% of its initial capacity. This does not mean that it has to be replaced, but as the battery ages, the risk of overheating or other types of failure increases.

Energy density Nominal battery energy divided by the battery volume. The same considerations apply as for the specific energy. It is typically specified when volume is of importance for the application.

Nominal voltage The characteristic operating voltage reported in the battery manual. It is typically close to the battery's mid-point voltage–the battery voltage measured at 50% SOC

Open-circuit voltage The potential difference measured when no load is applied. The open-circuit voltage is dependent on the SOC.

Power density Maximum power the battery is able to output divided by total battery volume. Useful for estimating how large a battery must be for certain power application.

Primary battery A primary battery is a battery that is not rechargable, in contrast to a secondary battery, which can be recharged and used multiple times.

Secondary battery A secondary battery is a battery that is rechargable, in contrast to a primary battery, which can only be used once until depleted.

Specific energy Nominal battery energy divided by the battery mass. It depends on the battery chemistry, but also on battery packaging. Since a large part of a battery pack is packaging it is much lower than the theoretical maximum value. It is typically specified when weight is of importance for the application.

Specific power Maximum power the battery is able to output divided by total battery mass. Of importance for applications where batteries must output large bursts of power for a short time.

State-of-charge The battery state-of-charge (SOC) is defined as the current time battery capacity given as a percentage of its maximum capacity.

Bibliography

1. DNV GL. *2018 Energy Transition Outlook - Global and Regional Forecast to 2050* (Høvik, Norway, Sept. 2018).
2. *2014 Energy and Climate Outlook* (MIT Joint Program on the Science and Policy of Global Change, Oct. 2014).
3. Diaz de la Rubia, T., Klein, F., Shaffer, B., Kim, N. & Lovric, G. *Energy Storage: Tracking the Technologies That Will Transform the Power Sector* (Deloitte, 2015).
4. International Renewable Energy Agency (IRENA). *Off-Grid Renewable Energy Solutions to Expand Electricity Access: An Opportunity Not to Be Missed* (Abu Dhabi, 2019).
5. Few, S., Schmidt, O. & Gambhir, A. *Electrical Energy Storage for Mitigating Climate Change* (Grantham Institute, July 5, 2016). https://granthaminstitute.atavist.com/electrical-energy-storage-technologies (2019).
6. Norsk elbilforening. *Ladeklart Norge 2025* (Mar. 2019). https://wpstatic.idium.no/elbil.no/2019/03/Ladeklart-Norge-2025.pdf.
7. EUROBAT. *Battery Energy Storage in the EU* (Association of European Automotive and Industrial Battery Manufacturers, 2017). https://eurobat.org/images/news/publications/eurobat_batteryenergystorage_web.pdf (2019).
8. Winter, M. & Brodd, R. J. What Are Batteries, Fuel Cells, and Supercapacitors? *Chemical Reviews* **104,** 4245–4270. ISSN: 0009-2665 (Sept. 28, 2004).
9. Georgia State University. *Table of Standard Electrode Potentials* http://hyperphysics.phy-astr.gsu.edu/hbase/Tables/electpot.html (2019).
10. Atkins, P., Atkins, P. W. & de Paula, J. *Atkins' Physical Chemistry* 10th ed. ISBN: 978-0-19-969740-3 (OUP Oxford, 2014).
11. *Linden's Handbook of Batteries* (eds Reddy, T. D. & Linden, D.) 4th ed. (McGraw Hill Professional, June 5, 2010). 1457 pp. ISBN: 978-0-07-162419-0.

12. Mayneord William Valentine. John Alfred Valentine Butler, 14 February 1899 - 16 July 1977. *Biographical Memoirs of Fellows of the Royal Society* **25,** 144–178 (Nov. 1, 1979).

13. Omar, N., den Bossche, P. V., Coosemans, T. & Mierlo, J. V. Peukert Revisited—Critical Appraisal and Need for Modification for Lithium-Ion Batteries. *Energies* **6,** 5625–5641 (Nov. 2013).

14. Jongerden, M. & Haverkort, B. R. *Battery Modeling CTIT Technical Report Series* **TR-CTIT-08-01** (Design and Analysis of Communication Systems (DACS), Jan. 2008).

15. Panasonic. *Eneloop AA 4-Pack* http://www.panasonicbatteryproducts.com/eneloop_rechargeable_batteries/eneloop_rechargeable_batteries-aa_4-pack/ (2019).

16. Young, K.-H. & Yasuoka, S. Capacity Degradation Mechanisms in Nickel/Metal Hydride Batteries. *Batteries* **2,** 3 (Mar. 1, 2016).

17. IRENA. *Electricity Storage and Renewables: Costs and Markets to 2030* (International Renewable Energy Agency, 2017).

18. Argyrou, M. C., Christodoulides, P. & Kalogirou, S. A. Energy Storage for Electricity Generation and Related Processes: Technologies Appraisal and Grid Scale Applications. *Renewable and Sustainable Energy Reviews* **94,** 804–821. ISSN: 1364-0321 (Oct. 1, 2018).

19. Gaines, L. The Future of Automotive Lithium-Ion Battery Recycling: Charting a Sustainable Course. *Sustainable Materials and Technologies* **1-2,** 2–7. ISSN: 2214-9937 (Dec. 1, 2014).

20. Heelan, J., Gratz, E., Zheng, Z., Wang, Q., Chen, M., Apelian, D. & Wang, Y. Current and Prospective Li-Ion Battery Recycling and Recovery Processes. *JOM* **68,** 2632–2638. ISSN: 1543-1851 (Oct. 1, 2016).

21. Lv, W., Wang, Z., Cao, H., Sun, Y., Zhang, Y. & Sun, Z. A Critical Review and Analysis on the Recycling of Spent Lithium-Ion Batteries. *ACS Sustainable Chemistry & Engineering* **6,** 1504–1521 (Feb. 5, 2018).

22. Nilar AB. *Nilar - Technical Manual NiMH Bi-Polar Battery Technology* Aug. 2018. http://www.nilar.com/wp-content/uploads/2017/08/Nilar-Energy-Storage-Technical-Manual.pdf (2018).

23. Gras, M. *Recycling of Metals from NiMH Batteries: Development of Liquid-Liquid Selective Extractions Based on Ionic Liquids* (Université Grenoble Alpes, 2018). https://tel.archives-ouvertes.fr/tel-01913113.

24. Shen, Y., Noréus, D. & Starborg, S. Increasing NiMH Battery Cycle Life with Oxygen. *International Journal of Hydrogen Energy. The 2nd International Symposium on Materials for Energy Storage and Conversion (mESC-IS2017)* **43,** 18626–18631. ISSN: 0360-3199 (Oct. 4, 2018).

25. Meng, T., Young, K.-H., Koch, J., Ouchi, T. & Yasuoka, S. Failure Mechanisms of Nickel-Metal Hydride Batteries with Cobalt-Substituted Superlattice Hydrogen-Absorbing Alloy Anodes at 50 °C. *Batteries* **2,** 20 (Sept. 2016).

26. Kong, L., Li, C., Jiang, J. & Pecht, M. G. Li-Ion Battery Fire Hazards and Safety Strategies. *Energies* **11,** 2191 (Sept. 2018).

27. Bandhauer, T. M., Garimella, S. & Fuller, T. F. A Critical Review of Thermal Issues in Lithium-Ion Batteries. *Journal of The Electrochemical Society* **158,** R1–R25. ISSN: 0013-4651, 1945-7111 (Jan. 3, 2011).

28. Seaman, A., Dao, T.-S. & McPhee, J. A Survey of Mathematics-Based Equivalent-Circuit and Electrochemical Battery Models for Hybrid and Electric Vehicle Simulation. *Journal of Power Sources* **256,** 410–423. ISSN: 0378-7753 (June 15, 2014).

29. Shepherd, C. M. Design of Primary and Secondary Cells II . An Equation Describing Battery Discharge. *Journal of The Electrochemical Society* **112,** 657–664. ISSN: 0013-4651, 1945-7111 (Jan. 7, 1965).

30. Raszmann, E., Baker, K., Shi, Y. & Christensen, D. *Modeling Stationary Lithium-Ion Batteries for Optimization and Predictive Control* in *2017 IEEE Power and Energy Conference at Illinois (PECI)* 2017 IEEE Power and Energy Conference at Illinois (PECI) (IEEE, Champaign, IL, USA, Feb. 2017), 1–7. ISBN: 978-1-5090-5550-0. DOI: 10.1109/PECI.2017.7935755.

31. Song, D., Sun, C., Wang, Q. & Jang, D. A Generic Battery Model and Its Parameter Identification. *Energy and Power Engineering* **10,** 10 (Jan. 12, 2018).

32. Doerffel, D. & Sharkh, S. A. A Critical Review of Using the Peukert Equation for Determining the Remaining Capacity of Lead-Acid and Lithium-Ion Batteries. *Journal of Power Sources* **155,** 395–400. ISSN: 0378-7753 (Apr. 21, 2006).

33. Duracell. *Cycle and Battery Life* https://web.archive.org/web/20010909125450/http://www.duracell.com/oem/Rechargeable/Nickel/cycbatlif.asp (2019).

34. Jiang, J., Shi, W., Zheng, J., Zuo, P., Xiao, J., Chen, X., Xu, W. & Zhang, J.-G. Optimized Operating Range for Large-Format LiFePO4/Graphite Batteries. *Journal of The Electrochemical Society* **161,** A336–A341. ISSN: 0013-4651, 1945-7111 (Jan. 1, 2014).

35. Ruiz, V. *Standards for the Performance and Durability Assessment of Electric Vehicle Batteries : Possible Performance Criteria for an Ecodesign Regulation.* EUR 29371 EN (Publications Office of the Euroean Union, Luxembourg, Oct. 12, 2018). DOI: 10.2760/24743.

36. Matsuishi, M. & Endo, T. Fatigue of Metals Subjected to Varying Stress. *Japan Society of Mechanical Engineers, Fukuoka, Japan* **68,** 37–40 (1968).

37. Shi, Y., Xu, B., Tan, Y. & Zhang, B. *A Convex Cycle-Based Degradation Model for Battery Energy Storage Planning and Operation* in *2018 Annual American Control Conference (ACC)* 2018 Annual American Control Conference (ACC) (June 2018), 4590–4596. DOI: 10.23919/ACC.2018.8431814.

38. HOMER Energy. *Modified Kinetic Battery Model* https://www.homerenergy.com/products/pro/docs/3.11/modified_kinetic_battery_model.html (2019).

39. Omar, N., Monem, M. A., Firouz, Y., Salminen, J., Smekens, J., Hegazy, O., Gaulous, H., Mulder, G., Van den Bossche, P., Coosemans, T. & Van Mierlo, J. Lithium Iron Phosphate Based Battery – Assessment of the Aging Parameters and Development of Cycle Life Model. *Applied Energy* **113,** 1575–1585. ISSN: 0306-2619 (Jan. 1, 2014).

40. Smith, K., Saxon, A., Keyser, M., Lundstrom, B., Cao, Z. & Roc, A. *Life Prediction Model for Grid-Connected Li-Ion Battery Energy Storage System* in *2017 American Control Conference (ACC)* 2017 American Control Conference (ACC) (May 2017), 4062–4068. DOI: 10.23919/ACC.2017.7963578.

41. Pesaran, A. A. Thermal Performance of EV and HEV Battery Modules and Packs, 11.

42. Tremblay, O., Dessaint, L.-A., Tremblay, O. & Dessaint, L.-A. Experimental Validation of a Battery Dynamic Model for EV Applications. *World Electric Vehicle Journal* **3,** 289–298 (June 26, 2009).

43. MathWorks Nordic. *Simulink* https://se.mathworks.com/help/simulink/ (2019).

44. Nilar AB. *Nilar EC Product Catalogue 2018* Apr. 2018. http://www.nilar.com/wp-content/uploads/2018/03/Nilar-EC-Product-catalogue-2018.pdf (2018).

45. Pesaran, A. & Keyser, M. *Thermal Characteristics of Selected EV and HEV Batteries* in *Sixteenth Annual Battery Conference on Applications and Advances. Proceedings of the Conference (Cat. No.01TH8533)* Sixteenth Annual Battery Conference on Applications and Advances. (IEEE, Long Beach, CA, USA, 2001), 219–225. ISBN: 978-0-7803-6545-2. DOI: 10.1109/BCAA.2001.905129.

46. Nicholas, M. & Hall, D. *Lessons Learned on Early Electric Vehicle Fast-Charging Deployments* (International Council on Clean Transportation, Washington, DC 20005 USA, July 2018), 54. https://www.theicct.org/publications/fast-charging-lessons-learned (2019).

47. Trentadue, G., Lucas, A., Otura, M., Pliakostathis, K., Zanni, M. & Scholz, H. Evaluation of Fast Charging Efficiency under Extreme Temperatures. *Energies* **11,** 1937 (Aug. 2018).

48. Kane, M. *Let's Look At Fast Charging Curves For Popular Electric Cars* https://insideevs.com/news/338777/lets-look-at-fast-charging-curves-for-popular-electric-cars/ (2019).

49. Heggen, H. & Lidal, R. *Seier nei til hurtigladar etter prissjokk* https://www.nrk.no/sognogfjordane/seier-nei-til-hurtigladar-etter-prissjokk-1.14532023 (2019).

50. Nilar AB. *Nilar EC Brochure 2019* Apr. 2019. http://www.nilar.com/wp-content/uploads/2019/04/Nilar-EC-Brochure-2019-EN.pdf (2019).